Astronomical control on marine anoxia during the Kellwasser Crisis and Rhinestreet Event (Appalachian Basin, New York, USA)

Jarno J.C. Huygh[1], Thomas J. Algeo[2,3,4], Bradley B. Sageman[5], Michiel Arts[1], Charles A. Ver Straeten[6], D. Jeffrey Over[7], Justin Gérard[8], Loïc Sablon[8], Michel Crucifix[8] and Anne-Christine Da Silva[1]

[1] SediCClim Laboratory, Department of Geology, Liège University, Liège, Belgium

[2] Department of Geosciences, University of Cincinnati, Cincinnati, OH, USA

[3] State Key Laboratory of Geomicrobiology and Environmental Changes (GMEC), China University of Geosciences, Wuhan, China

[4] State Key Laboratory of Oil and Gas Reservoir Geology and Exploitation, Institute of Sedimentary Geology, Chengdu University of Technology, Chengdu, China

[5] Department of Earth, Environmental and Planetary Sciences, Northwestern University, Evanston, IL, USA

[6] New York State Museum, Albany, NY, USA

[7] Department of Geological, Environmental, and Planetary Sciences, SUNY Geneseo, Geneseo, NY, USA

[8] Earth and Life Institute, UCLouvain, Louvain-la-Neuve, Belgium

Corresponding author: Jarno Huygh (jarno.huygh@uliege.be)

Abstract

The Kellwasser Crisis near the Frasnian-Famennian boundary (~372 Ma) is linked to one of the major Phanerozoic biodiversity crises. It is associated with sea-level changes, carbon-cycle perturbations, and pulsed oceanic anoxia, that led to black shale deposition characterized by positive carbon isotope excursions, akin to the Kellwasser horizons in Germany. Despite growing evidence of astronomically forced climatic stresses influencing Devonian marine systems, the trigger mechanism(s) of the Kellwasser Event remain debated. The West Valley core (WVC) comprises middle Frasnian to lower Famennian strata, including the Rhinestreet and Kellwasser events, characterized by black shales, elevated total organic carbon (TOC) content, and a positive $\delta^{13}C_{org}$ carbon isotope excursion in the Kellwasser Crisis interval. In this work, we performed cyclostratigraphic analysis of Ti, Ti/Al and TOC, which reveals a strong astronomical imprint, particularly eccentricity amplitude modulation patterns. The TOC record was tuned to the stable 405-kyr eccentricity period, yielding a 5.67-Myr-long floating astrochronology, with event durations for the Rhinestreet and Kellwasser intervals consistent with previous reports. Subsequent analysis confirmed an equally strong eccentricity imprint on the titanium content, strongly implying a link between organic matter preservation, detrital sediment supply and astronomical forcing. Additionally, a dominant imprint of the 1.2-Myr and 2.4-Myr obliquity cycles on sea-level variation supports astronomical control on the Kellwasser Crisis. Finally, new insights into the phase relationship between the Rhinestreet and Kellwasser events and astronomically forced climate changes are globally contextualized within a new cyclostratigraphic model, emphasizing the role of eccentricity and obliquity in pacing marine anoxia.

Keywords: cyclostratigraphy; Devonian; Frasnian-Famennian boundary; West Valley core; black shale; orbital forcing

1. Introduction

The Kellwasser Crisis interval is one of the “big five” mass extinction events in Earth’s history (Raup and Sepkoski; 1982; Schindler, 1990; 1993). It was a period of increased climate instability, marine biodiversity loss and pulses of marine anoxia, culminating during the Lower Kellwasser (LKW) Event and Upper Kellwasser (UKW) Event at the Frasnian-Famennian (F-F) boundary (Walliser, 1996; Carmichael et al., 2019; Becker et al., 2020; Brett et al., 2020). The Kellwasser Crisis is associated with positive carbon isotope excursions (pCIE), eustatic sea-level change (e.g., transgressive-regressive pulses), and deposition of organic-rich strata (Becker et al., 2020). Yet Carmichael et al. (2019) highlighted that, despite a considerable sampling bias, the expression of the Kellwasser Crisis in the geological record is highly dependent on paleoenvironment and paleogeography. In addition to the severe Kellwasser Crisis, the Rhinestreet (RS) Event, named after black shale deposits in New York, USA (Lash and Blood, 2006) was a minor bio-event of low severity (Brett et al., 2020) that nonetheless represents a global event associated with transgression, marine anoxia and deposition of organic-rich facies (Sageman et al., 2003; Lash and Blood, 2006; Becker et al., 2020; Kabanov et al., 2023).

Marine anoxia is often attributed to water-column stratification caused by stagnation of the ocean circulation, or to enhanced productivity in upwelling zones or epeiric seas, which leads to eutrophication, and ultimately results in anoxia (Murphy et al., 2000; Carmichael et al., 2019; Kabanov et al., 2023; Algeo and Shen, 2024). Alternative explanations also point to vertical chemocline displacement, particularly during transgression (see reviews in Carmichael et al., 2019; Kabanov et al., 2023). These mechanisms represent the environmental response (i.e., proximal causes) to changes in redox chemistry and temperature, which are, in turn, related to a perturbation of the (global) carbon cycle (Algeo and Shen, 2024). Biocrises linked to organic carbon burial (i.e., pCIE), atmospheric CO_2 drawdown, and climatic cooling are typically driven by weathering and productivity changes, whereas those linked to carbon release (i.e., negative CIE), atmospheric CO_2 rise, and climatic warming are generally temperature-driven (Algeo and Shen, 2024).

The ultimate causes behind the most severe mass extinctions include bolide impacts, large igneous province (LIP) volcanism, tectono-oceanic events, or bioevolutionary events (Kabanov et al., 2023; Algeo and Shen, 2024). Even though ongoing orogeny (e.g., Averbuch et al., 2005) or LIP volcanism (e.g., Pisarzowska and Racki, 2020; Racki, 2020) have been proposed as the triggering mechanism behind the Kellwasser Crisis (see also Carmichael et al., 2019; Kabanov et al., 2023), its ecological scope, protracted multistage nature and characteristic positive carbon cycle response – indicating net carbon burial and associated cooling – points to a bioevolutionary trigger as the ultimate cause (Algeo and Shen, 2024). In addition, the conspicuous temporal link with the expansion of land plants (Algeo and Scheckler, 1998, 2010) further substantiates a connection between the mass extinction, associated anoxia, and land-plant-mediated changes in carbon burial and continental weathering ('land-plant weathering' hypothesis; Algeo et al., 1995).

Recent work on Devonian cyclostratigraphy suggests that astronomical forcing, in interplay with other factors, played a key role in the timing and pacing of the Kellwasser marine anoxia episodes (De Vleeschouwer et al., 2017; Da Silva et al., 2020; Lu et al., 2021; Ma et al., 2022; Wichern et al., 2024). Moreover, recent modelling efforts using an Earth system model of intermediate complexity (cGENIE) revealed that astronomical forcing, primarily obliquity variation, is able to drive changes in ocean oxygenation and impact marine anoxia by altering both circulation and oxygen solubility (Gérard et al., 2025). Astronomical forcing refers to changes in the amount and distribution of insolation caused by variations in Earth's orbital parameters and obliquity, driven by gravitational interactions with other celestial bodies, including luni-solar precession. In the classical theory of planetary motion, the precession of the planet's perihelion in the reference frame, modulated by eccentricity, has characteristic frequencies g_i, and the precession of the orbital plane around the reference frame, modulated by inclination, has characteristic frequencies s_i (e.g., Bretagnon 1974, Laskar, 1990). The key factors controlling the distribution of insolation are the obliquity of the equator with respect to the orbital plane, and the eccentricity-modulated precession of the perihelion with respect to Earth's position at the vernal equinox. To obtain these two quantities, one must combine the orbital model with a model of luni-solar precession, largely described by a movement of frequency *k*. Obliquity is mainly dominated by the s_i+k terms, climatic precession by the g_i+k terms, and eccentricity – the envelope of climatic precession – by differences in the g_i terms (Berger, 1973). These are commonly referred to as the Milankovitch cycles, which affect Earth's insolation and climate and, if amplified and preserved, can be found imprinted in the sedimentary record (Hinnov, 2000).

Cyclostratigraphy leverages the recognized imprint of Milankovitch cycles, enabling the construction of high-resolution (floating) astrochronologies. This way, the duration of the WVC Rhinestreet Event, as well as the Kellwasser Crisis interval LKW and UKW events can be estimated. Additionally, the temporal location of these events relative to extrema in astronomical cycles can be investigated and documented. To date, two models have been proposed that describe the link between Milankovitch cycles and the LKW and UKW events. The eccentricity-minimum hypothesis proposes the presence of a 2.4-Myr minimum in eccentricity (i.e., 'node') before the UKW Event (De Vleeschouwer et al., 2017, Da Silva et al., 2020; Wichern et al., 2024). Such a minimum, characterized by limited modulation of precession by eccentricity, could favor stable climatic conditions allowing for the buildup of nutrients on the continent (nutrient-gun hypothesis; De Vleeschouwer et al., 2024), facilitated by the evolution and colonization of land plants (Algeo and Scheckler, 1998). After the node, the increase in eccentricity-modulated precession would intensify nutrient runoff and cause subsequent eutrophication and anoxia (De Vleeschouwer et al., 2024). Alternatively, Ma et al. (2022) proposed that both LKW and UKW were associated with an orbital configuration of high obliquity and eccentricity. Accordingly, significantly increased seasonality would, in turn, lead to enhanced nutrient input and sea-level rise, leading to eutrophication and anoxia (Ma et al., 2022). Regardless, both models suggest that the anoxia onset is climate-driven (proximate cause; Algeo and Shen, 2024). These models are complementary with the ‘weak version’ of the land-plant weathering hypothesis (Algeo and Shen; 2024); land-plant bioevolutionary events inducing considerable environmental stress, bringing the Earth system closer to a tipping point towards marine anoxia, with Milankovitch forcing providing the final contribution towards episodic marine anoxia and extinction (De Vleeschouwer et al., 2024). The impact of eustatic sea-level oscillations and ocean circulation changes on anoxia development during the Kellwasser Crisis have not yet been formulated within a cyclostratigraphic context.

Still, due to diverging cyclostratigraphic interpretations (e.g., De Vleeschouwer et al., 2017; Ma et al., 2022), the temporal history of the Kellwasser Crisis interval and its relationship with astronomically forced paleoclimatic and paleoenvironmental change remain debated. Additional sections containing the Kellwasser Crisis interval need to be investigated to provide new temporal estimates of the crisis interval and to test current models for astronomically forced marine anoxia. Building upon a long history of research on the Devonian of the Appalachian Basin, this work presents a cyclostratigraphic interpretation of cyclicity observed in the West Valley core (WVC), further refining work carried out by Murphy et al. (2000), Sageman et al. (2003) and Ver Straeten et al. (2011). In complement, a re-assessment of the geochemical data is carried out to establish the paleoclimatic and paleodepositional conditions of WVC strata within a cyclostratigraphic framework.

Even though the cyclicity captured by this record has been explicitly described within a sequence stratigraphic framework (e.g., Ver Straeten et al., 2011), no temporal framework based on Milankovitch cyclicity has been reported to date. First, the presence of an astronomical imprint in geochemical proxy series is leveraged for the construction of an astronomical age model. This way, the time encompassed by the WVC strata, as well as the Rhinestreet, LKW and UKW event beds is estimated. Next, the mechanisms (i.e., paleoclimatic and paleoenvironmental response) translating astronomically forced insolation changes into the WVC strata are put into a cyclostratigraphic context. Finally, the phase relationship between recovered Milankovitch cycles and the Rhinestreet, LKW, and UKW event beds is documented, formalized into a new model, and compared to current hypotheses.

2. Geological setting

The 260-m-thick western New York Nuclear Fuel Service core #1 or West Valley core NX-1 was drilled by the Western New York Nuclear Fuel Service near the town of Ashford (42.35306 °N, 78.67383 °W) in Cattaraugus County, New York State (USA) (Fig. 1A). It comprises middle Frasnian to lower Famennian distal foreland basin strata deposited in an expanded subtropical zone at appr. 30 °S paleolatitude (Ver Straeten et al., 2020), as the Catskill Delta prograded westward into the Appalachian foreland basin as a result of the Acadian Orogeny (Ver Straeten, 2009; 2010; Smith and Jacobi, 2023). During deposition of WVC strata, alongside eustatic sea-level variations, tectonic processes related to the ongoing orogeny (Tectophase 4 of Ver Straeten, 2023) exerted additional influence on relative sea-level through flexural adjustments, subsidence, and rebound (Ver Straeten, 2009; 2010; 2023).

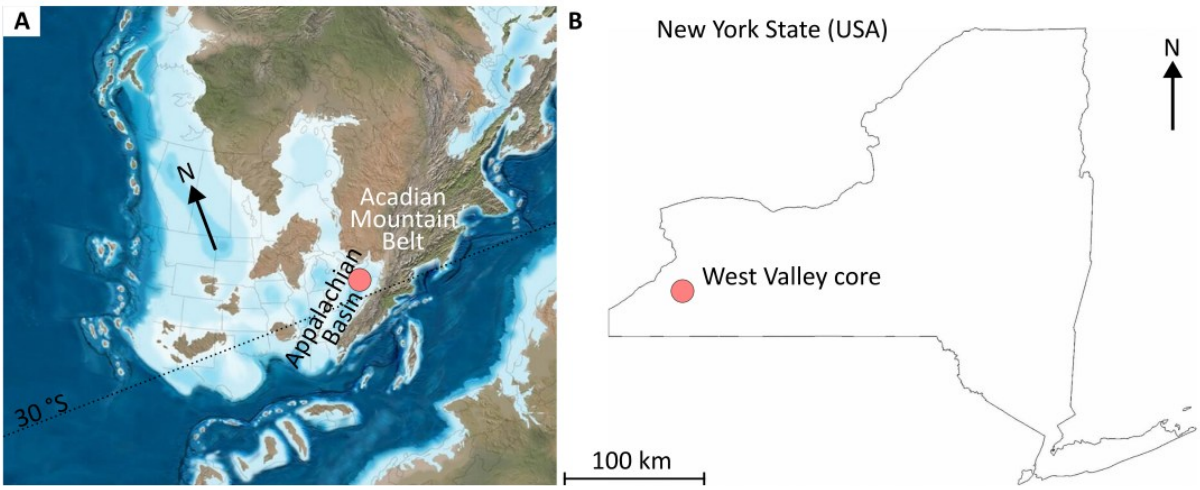

Fig. 1. Geological setting of the WVC. A) Late Devonian paleogeographic map (Blakey, 2023; 373 Ma). B) New York State (USA) modified from d-maps.com. WVC locality is indicated by a red dot.

From base to top, the WVC contains the black shales of the Rhinestreet Formation, mudstones intercalated with black shale of the Angola Formation, the mudstone to sandstones of the Gardeau and West Hill formations, the black shales of the Pipe Creek Formation, mudstones intercalated with black shale of the Hanover Formation, black shales and mudstones of the Dunkirk Formation and, the shales and mudstones of the South Wales Formation (Gowanda Formation in Ver Straeten et al., 2011) (Fig. 2). The contact between the Rhinestreet Formation and the underlying Cashaqua Formation is missing, indicating that the lowermost Rhinestreet Formation is absent in the WVC (Sageman et al., 2003; Ver Straeten et al., 2011). Identification of the LKW (Pipe Creek Formation) and UKW (Point Gratiot Bed-equivalent) events in western New York was based on conodont biostratigraphy (Over, 1997; Over et al., 2023), increased total organic carbon and a positive carbon isotope excursion (Murphy et al., 2000).

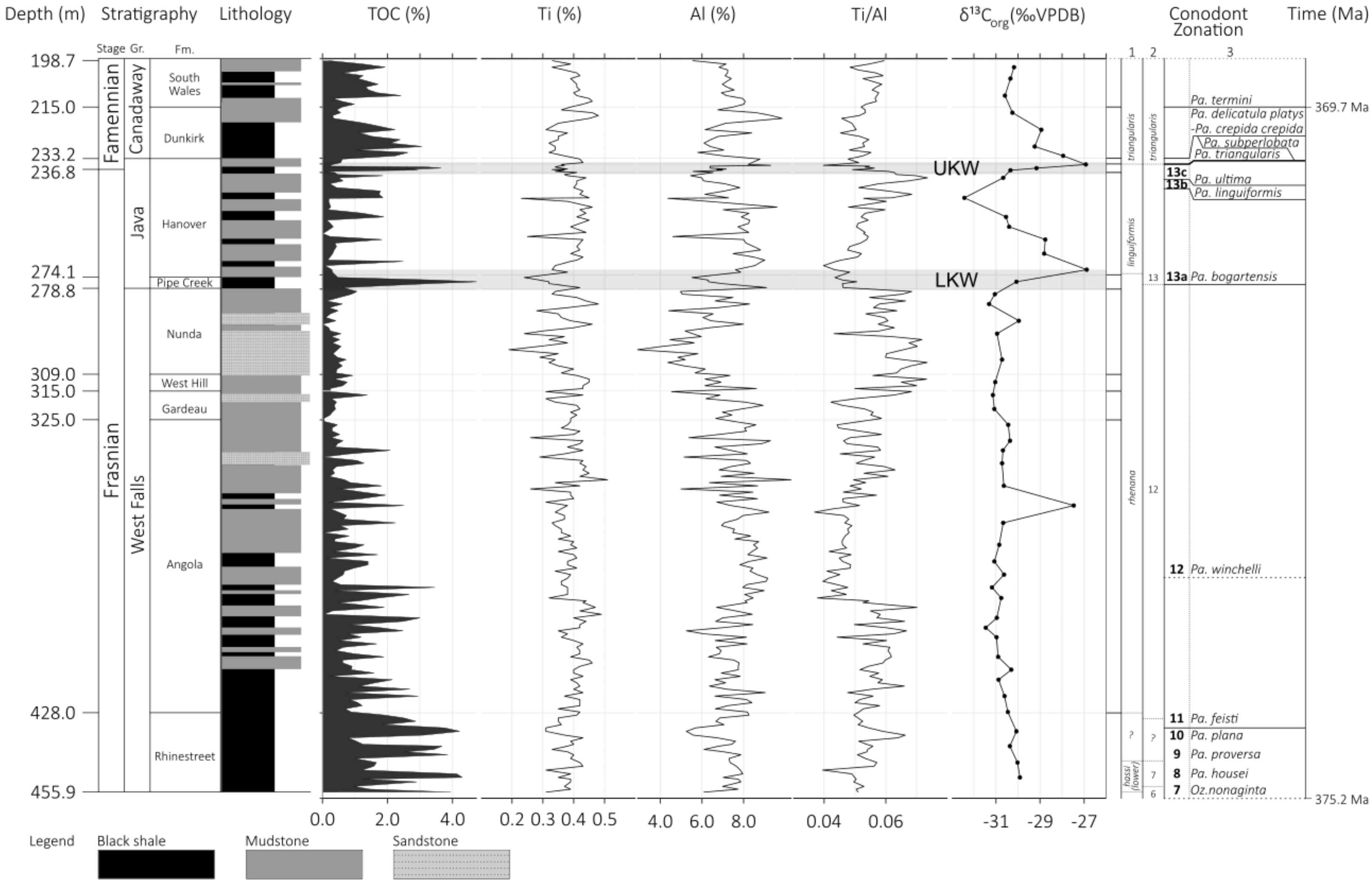

Fig. 2. WVC stratigraphy, lithological column, selected geochemical proxy signals and conodont zonation. Stratigraphy and lithological column modified after Ver Straeten et al. (2011). Geochemical proxy signals TOC, Ti, Al, Ti/Al and $\delta^{13}C_{org}$ from Sageman et al. (2003). Conodont zonation correlation based on Sageman et al. (2003) (1), Ver Straeten et al. (2011) (2) and Klapper and Kirchgasser (2016) and Over et al. (2023) (3). Numerical ages estimated based on correlation to conodont zonation by Becker et al. (2020).

3. Materials and methods

Geochemical proxy records used for cyclostratigraphy in the present study were published in Murphy et al. (2000) and Sageman et al. (2003), as was also the methodology for the acquisition of these. Here, emphasis is put on a specific set of proxies, primarily selected based on principal component analysis (PCA; Fig. 3.); total organic carbon (TOC; preserved organic matter), Ti (coarse-grained detrital influx; Croudace and Rothwell, 2015), Ti/Al (sea-level; Sageman et al., 2003) and stable carbon isotopes of organic matter ($\delta^{13}C_{org}$), as well as redox-sensitive proxies Ni enrichment factor (Ni_{EF}), Mo/Al, V/Al (Algeo and Liu, 2020), P (Murphy et al., 2000; Sageman et al., 2003; Percival et al., 2020) and Mo/TOC (Algeo and Lyons, 2006). Enrichment of Ni was calculated as: $Ni_{EF} = [(Ni/Al)_{sample}/(Ni/Al)_{upper\ crust}]$ according to McLennan (2001) using Al_{crust} = 8.04% and Ni_{crust} = 44 ppm.

Furthermore, the lag-1 autocorrelation coefficient (ρ_1), a measure for sedimentary noise, is included as a proxy for sea-level change (Meyers and Hinnov, 2010). Lower relative sea-level would induce increased sedimentary noise (see Mudelsee, 2010), which is reflected by a decrease in ρ_1-values (and vice-versa) (Li et al., 2018). Here, sedimentary noise recorded by TOC and Ti/Al is estimated by $\rho_{1,\ TOC}$ and $\rho_{1,\ Ti/Al}$, respectively (see R script in Suppl. A). These proxies are utilized, either as time series for cyclostratigraphic analysis and/or as a complement for synthesizing a paleoclimatic interpretation.

Statistical treatment and analyses were carried out in RStudio (2024.12.1, Build 563). Cyclostratigraphic analyses were carried out in RStudio using the Astrochron v1.4 package (Meyers, 2014). Additional analysis using continuous wavelet transform with a Morlet wavelet (ω = 6) was carried out using the WaverideR package (Arts, 2023; Arts et al., 2024). The Nadaraya–Watson kernel regression estimate was calculated via the ‘ksmooth’ function. Proxy time series were detrended, either by subtracting a linear trend using the ‘detrend’ function or by fitting and removing a ‘lowess’ smoother using the ‘noLow’ function (Meyers, 2014). All proxy time series were linearly interpolated (0.25 m sampling rate) prior to carrying out any cyclostratigraphic analysis. TimeOpt and eTimeOpt (Astrochron; Meyers, 2015; 2019) were utilized to estimate the average and evolutive apparent sedimentation rate (ASR), respectively. Estimation of sedimentation rate is carried out by simultaneously optimizing (i) the modulation of the short-eccentricity cycle by the long-eccentricity cycle, and (ii) the concentration of spectral power at the periods of short-eccentricity (appr. 95, 99, 125, and 131 kyr) and long-eccentricity (405 kyr) (i.e., estimating r^2_{opt}; Meyers, 2015; 2019). The formulated cyclostratigraphic hypothesis and proposed astrochronology is subsequently tested by applying time series and spectral analyses on time-domain geochemical proxy signals. Specific focus is put on amplitude modulation patterns of eccentricity and obliquity cycles by extracting higher-order cycles from the envelope of hierarchically shorter cycles. To avoid convoluted phrases, LE(i) is used to denote the '405-kyr-long eccentricity cycle, recovered indirectly (i) from the envelope of the 100-kyr-short-eccentricity (SE) cycle'. Similarly, GE(i) and GO(i) are used for the indirectly recovered 2.4-Myr grand-eccentricity and 1.2-Myr grand-obliquity cycles, recovered from the envelopes of LE and 173-kyr long-obliquity (LO), respectively. All R-code is available in the Supplementary Materials (Suppl. A).

4. Results

4.1. Principal component analysis of geochemical data

While the geochemical framework of the WVC has been previously characterized by Murphy et al. (2000), Sageman et al. (2003), Ver Straeten et al. (2011), and briefly by Percival et al. (2020), a re-evaluation of the dataset using PCA is warranted to refine proxy selection and interpretation – particularly in light of recent advances in redox-proxy evaluation (Algeo and Liu, 2020). While principal component 1 (PC1) accounts for 30.4% of variance, PC2 and PC3 account for 18.8% and 14.2% of variance, respectively (Fig. 3). Most elements are grouped off-axis in PC1-PC2 space, with four distinct clusters of elements each occupying one of the quadrants: Ca, P and Mn (upper left), Fe, Al, Cr, K and Ti (upper right), V, Cu, Ni, Mo and TOC (lower right) and, Co, Si, Zr (lower left) (Fig. 3A). As such, PC1 and PC2 primarily reflect changes in detrital input and redox conditions, respectively (Fig. 3A). Grouping of elements such as Si, Zr and Ti (coarse-grained particles), Fe, Al, Cr, K, V and Co (finer, clayrich sedimentation), and associations between TOC, Mn, Mo, Cu and Ni (redox-sensitive organic-rich facies) along PC3 (Fig. 3A) suggests clustering as a function of grain size or sedimentological differences (Tribovillard et al., 2006; Croudace and Rothwell, 2015; Algeo and Liu, 2020, Tribovillard, 2021). Consequently, only a minority of the datapoints can be associated with the carbonate-containing fraction (i.e., Ca; blue data points on Fig. 3B) – consistent with the predominant mudstone, shale and sandstone facies of the WVC.

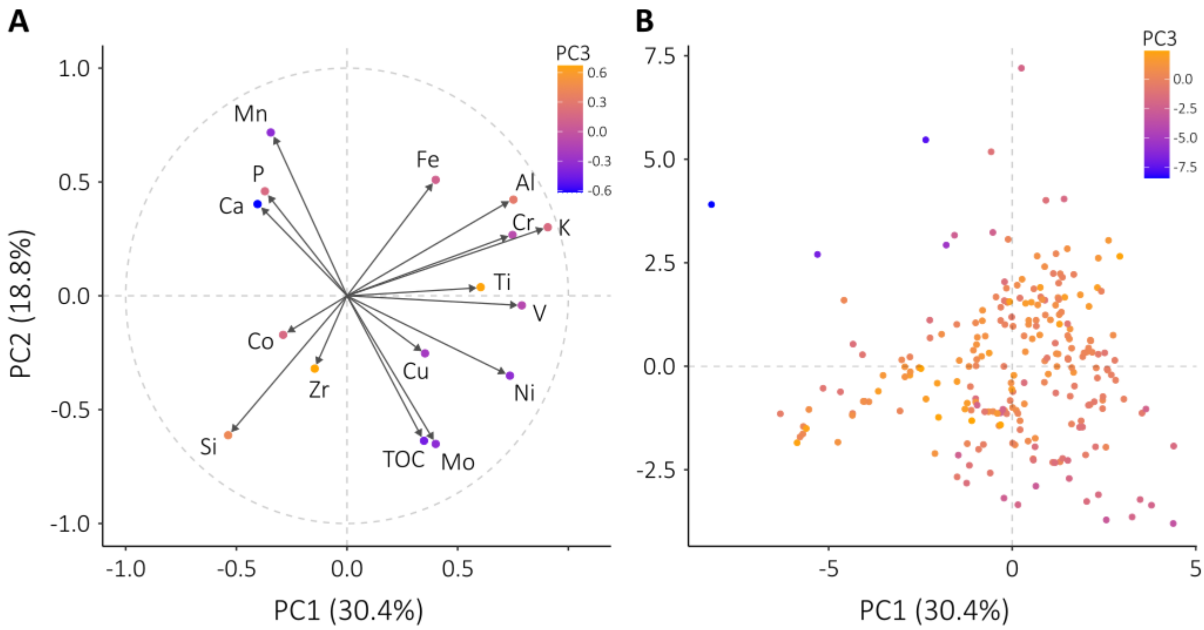

Fig. 3. Principal component analysis. A) Loading plot of selected elements along PC1, PC2 and PC3 (color scale). B) Score plot along PC1, PC2 and PC3 (color scale). PC3 accounts for 14.2% of variance.

4.2. Depth-domain cyclostratigraphy

Throughout the WVC, TOC spikes appear rhythmically, superimposed on a fluctuating baseline (Fig. 2). These are visually most striking within the Kellwasser Crisis interval (appr. 236 to 283 m), but also Rhinestreet, Angola, Dunkirk and South Wales formations. Time series analysis using a Nadaraya–Watson kernel regression estimate fit reveals apparent rhythmicity in the TOC baseline (Fig. 4A). Similarly, rhythmicity can also be observed in the Ti baseline (Fig. 4C).

In order to identify the presence of Milankovitch cyclicity imprinted on the TOC and Ti, spectral analysis was applied using a continuous wavelet transform (Arts, 2023; Arts et al., 2024). Increased wavelet power can be observed for two components with periodicities ranging from 4 to 8 m and 15 to 30 m, respectively (black dotted lines, Fig. 4B, D). Slight shifts in periodicity can be identified on the wavelet spectra (Fig. 4B, D) for both identified components, which may reflect changes in the ASR.

A Taner bandpass filter (window size of 1/30 to 1/15 m^{-1}) was used to extract the low-frequency component, identified in the wavelet spectra, from the TOC and Ti signals. In both cases, the bandpass filtered signals match the Nadaraya–Watson kernel regression estimates (Fig. 4A, C), confirming that the rhythmic changes in the TOC and Ti baselines are cyclic. Moreover, the low-frequency components extracted from TOC and Ti appear anti-phased. Secondly, the 4 to 8 m component is extracted using a bandpass filter. It fits with the sharp TOC (and Ti) spikes that can be observed most clearly in the Kellwasser Crisis interval (230 to 280 m, Figs. 2, 4).

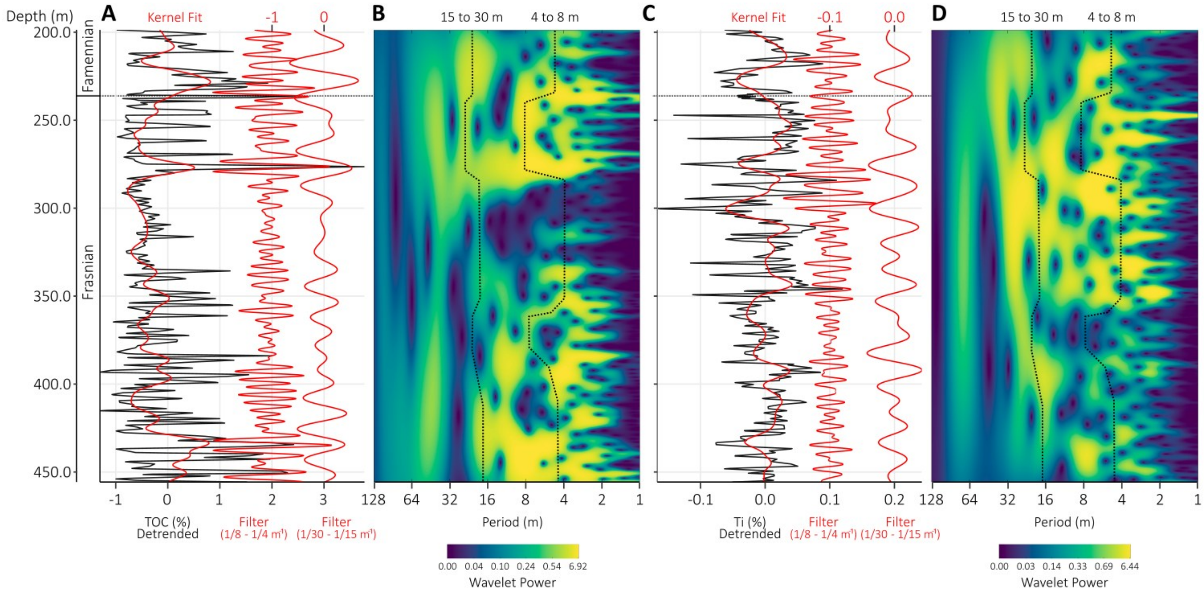

Fig. 4. WVC TOC and Ti, depth-domain time series and spectral analysis. A) Detrended TOC (%; black), Nadaraya–Watson kernel regression estimate (red) and bandpass filtered output (1/30 to 1/15 m^{-1} and 1/8 to 1/4 m^{-1}; red). B) TOC wavelet power with indicated periodicities from 15 to 30 m and 4 to 8 m, interpreted to correspond to the long- and short-eccentricity cycles, respectively. C) Detrended Ti (%; black), Nadaraya–Watson kernel regression estimate (red) and bandpass filtered output (1/30 to 1/15 m^{-1} and 1/8 to 1/4 m^{-1}; red). D) Ti wavelet power with indicated periodicities from 15 to 30 m and 4 to 8 m, interpreted to correspond to the long- and short-

eccentricity cycles, respectively. The cone of influence was removed from the wavelet periodograms for visual clarity (see Suppl. A).

4.3. Astronomical age model

Published conodont zonation biostratigraphy offers an independent age model for the WVC (Fig. 2; see also Sageman et al., 2003; Ver Straeten et al., 2011; Becker et al., 2020). Based on tentative correlations to generalized conodont zonation (Klapper and Kirchgasser, 2016; Becker et al., 2020; Over et al., 2023), the approximate amount of time encompassed by the WVC strata is roughly 5.5 Myr (Klapper and Kirchgasser, 2016; Becker et al., 2020) and accordingly, the ASR for the WVC is about 4.7 cm/kyr. At this rate, the 405-kyr long-eccentricity (LE) cycle would span on average 18.9 m. This suggests that the long-term periodic 15 to 30 m component that was identified in both TOC and Ti (Fig. 4) corresponds to the LE cycle. Similarly, the short-term periodic 4 to 8 m component most likely corresponds to the ~100-kyr SE cycle. The periods of these components also exhibit a 1:4 ratio akin to that between the long- and short-eccentricity cycles.

TimeOpt analysis (testing ASRs from 1 to 7 cm/kyr) estimates an average ASR of 4.75 cm/kyr (r^2_{opt} TOC) and 3.86 cm/kyr (r^2_{opt} Ti), well in line with biostratigraphic estimates (e.g., Becker et al., 2020). Furthermore, eTimeOpt (from 1 to 7 cm/kyr) is applied to TOC and Ti in order to assess potential changes in ASR as suggested by the continuous wavelet transform (Fig. 4). In both cases, eTimeOpt confirms previously estimated ASRs as well as the stratigraphic location of main shifts in ASR (r^2_{opt}) (see Fig. S1).

Integration of biostratigraphy and cyclostratigraphy strongly suggests an imprint of the short- and long-eccentricity cycles on TOC and Ti. Because TOC reflects the clearest apparent Milankovitch imprint (in terms of bundling and pacing of sharp spikes superimposed on the fluctuating baseline), this signal is used to construct an astronomical age model. Using the extracted long-eccentricity signal (Fig. 4A) as a guide, 14 local extrema in the TOC signal are visually identified and utilized to construct a floating astrochronology (i.e., minimal tuning on the LE cycle), encompassing 5.67 Myr at an average ASR of 4.53 cm/kyr (as illustrated in Fig. 5).

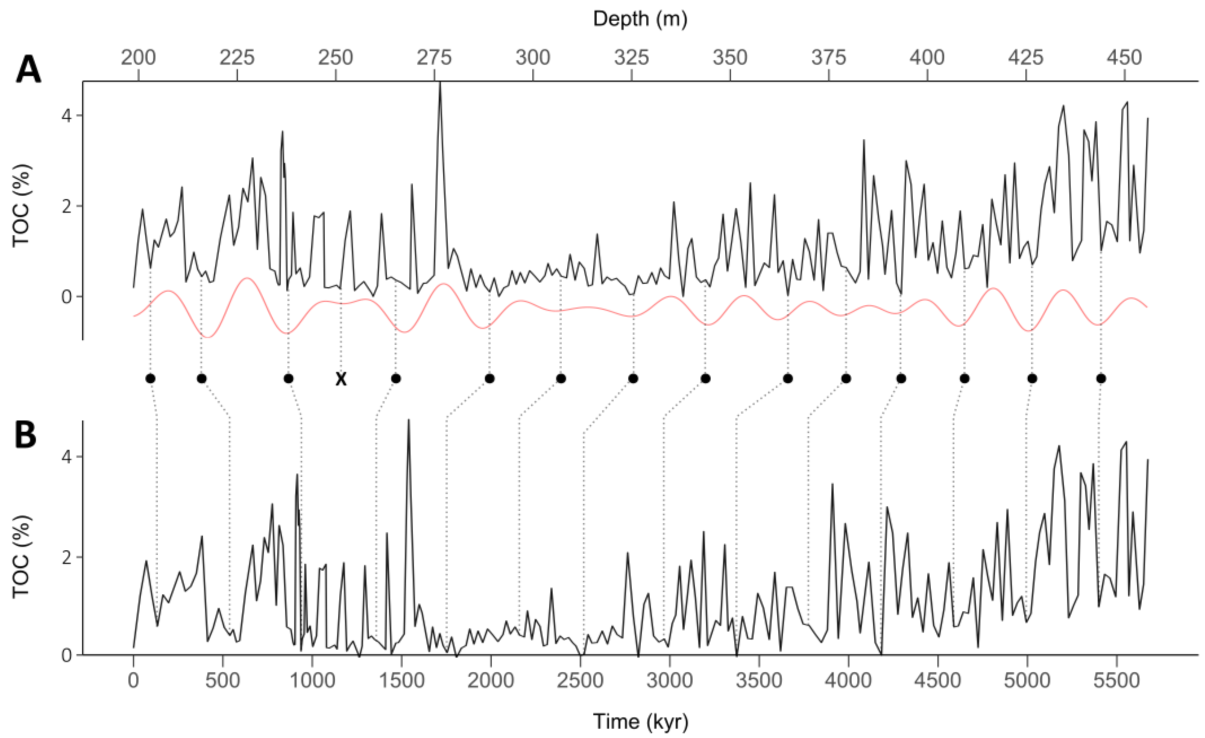

Fig. 5. Tuning of TOC using the 405-kyr LE cycle. A) Depth-domain TOC and bandpass filter output (1/30 to 1/15 m^{-1}) interpreted to reflect 405-kyr LE. B) Tuned, relative time-domain TOC. Dots reflect interpreted extrema in LE and are depth-time tie-points utilized to construct the age model. X reflects a potential additional extremum in LE which, after investigation, was not added for constructing the age model (see Suppl. Fig. S2).

Based on the interpreted imprint of eccentricity on TOC, the astronomical age model is used to transform all available geochemical proxies from the depth domain to the time domain. Note that at these estimated ASRs, recovery of precession (and short obliquity) is impeded by the limited resolution of the available geochemical dataset. So, the paleoclimatic response to astronomical forcing on short 10^4-yr timescales cannot be further investigated. Because statistical significance testing remains a debated subject within the cyclostratigraphy community (e.g., Weedon, 2022; Smith, 2023), a different approach is followed here by leveraging specific frequency ratios and amplitude modulation patterns that can be expected from longer-term (10^5-yr timescales) obliquity and eccentricity cycles. Note that both 1.2-Myr (s_4-s_3) and 2.4-Myr (g_4-g_3) cycles are unstable (Laskar, 2020) and that frequency ratios related to these cycles may diverge accordingly. In addition, the astronomical age model is tested by assessing the imprint of Milankovitch cycles on other proxies (that were tuned using the TOC age model).

4.4. Time-domain cyclostratigraphy

4.4.1. Organic matter (TOC)

In a first step, the imprint of Milankovitch cycles on the tuned TOC signal (Fig. 6A) is verified and documented. Continuous wavelet transform analysis reveals increased spectral power corresponding to LE and also at periodicities corresponding to SE, GE, LO, and GO (Fig. 6B). Notably, decreased SE spectral power can be observed around appr. 2.00 Myr (Nunda Formation) and 4.50 Myr (base of the Angola Formation) (Fig. 6), tentatively indicating the presence of a node (i.e., 2.4-Myr GE cycle minimum), during which the amplitude of SE is expected to be minimal (Laskar, 2020). Spectral power associated with GE remains moderate throughout the record, as expected given its low amplitude in Earth's eccentricity (Laskar, 2020). Spectral power associated with LO is strongly localized; primarily in the Rhinestreet Formation (appr. 5.00 to 5.67 Myr) but also in the LKW Event interval (appr. 1.40 to 1.80 Myr; Fig. 6B). As expected, increased GO spectral power is equally documented for the Rhinestreet Formation and, to a smaller extent, the overlying black shales of the lower Angola Formation (up to appr. 3.80 Myr; Fig. 6B).

In a second step, Taner bandpass filtering and Hilbert transforms are utilized to extract identified Milankovitch cycles and to assess their amplitude modulation patterns, respectively (Fig. 6A). Overall, bundles of 4 SE cycles can be counted per LE cycle, illustrating the expected 4:1 frequency ratio. A consistent in-phase relationship is documented between SE amplitude modulation patterns (and LE(i) on Fig. 6A) and the extracted LE cycle. An alternative age model, including an additional 405-kyr LE cycle in the Kellwasser interval, was discarded after displaying clear discrepancies in amplitude modulation patterns and cycle counting (see Fig. S2). Similar to SE and LE, the imprint of the GE cycle on TOC is investigated and documented. Extraction of the 2.4-Myr GE cycle is somewhat challenging due to the relatively short duration of the record (5.67 Myr), minor amplitude modulation observed for the recovered LE cycles (see GE(i), Fig. 6A), and the low amplitude and unstable nature of the g_4-g_3 term (Laskar, 2020). In this case, definite recovery of the exact temporal location of GE cycle extrema based on 1 proxy remains uncertain. Lastly, the fluctuating power of LO and GO (Fig. 6B) is visualized using bandpass filtering. Even though, overall, a frequency ratio of 7:1 LO to GO cycles is respected, a mismatch can be observed between GO(i) and GO (Fig. 6A). This is attributed to the weak imprint of obliquity on TOC in the Gardeau, West Hill, and Nunda formations, causing discrepancies in phasing. To conclude, a pronounced imprint of eccentricity on TOC has been documented. Conversely, strong evidence for obliquity control on TOC is lacking, except for the Rhinestreet Formation (Fig. 6). A highly similar analysis of Ti as described for TOC, corroborates the proposed astronomical interpretation (Fig. S3).

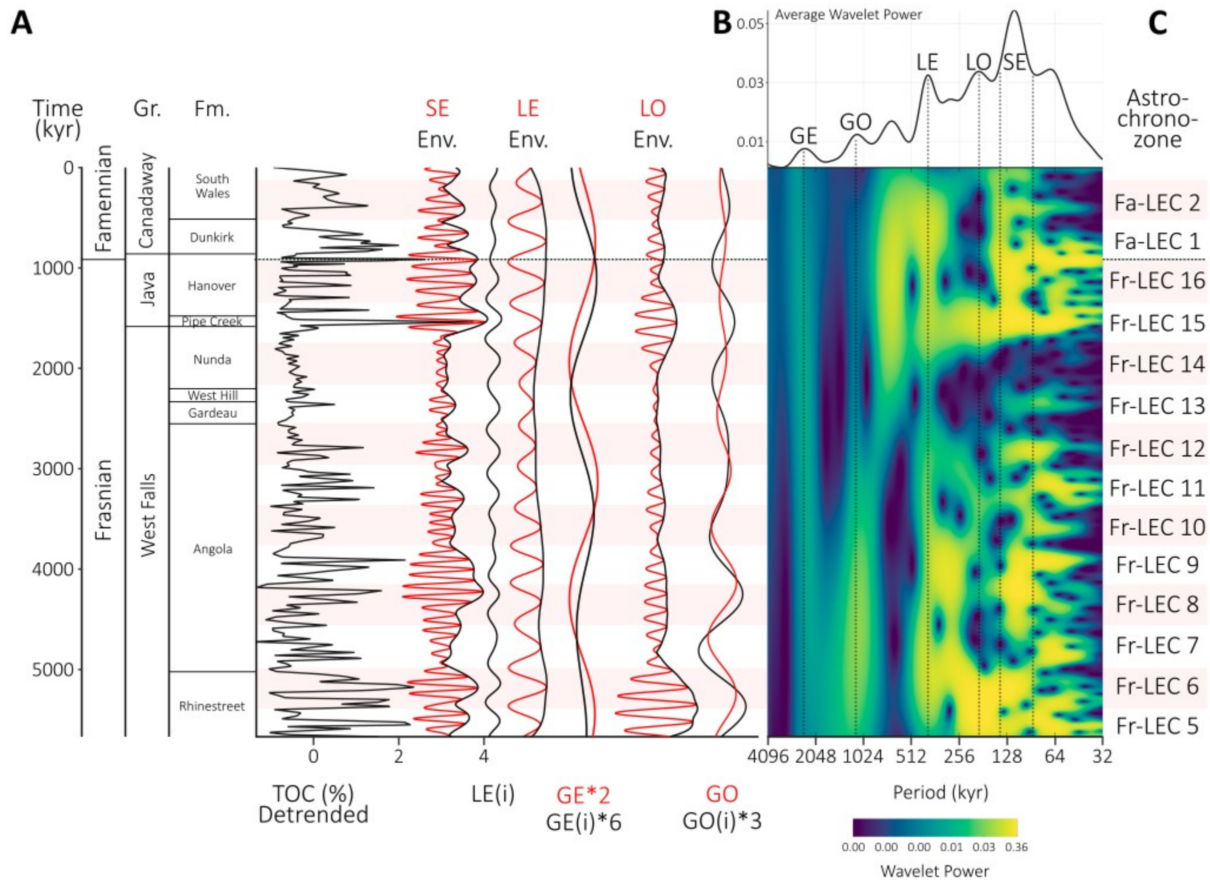

Fig. 6. Time-domain cyclostratigraphic analysis of TOC. A) WVC Stratigraphy: Stage, Group (Gr.) and Formation (Fm.), detrended TOC and bandpass filters corresponding to ~100-kyr SE (red; 1/150 to 1/80 kyr^{-1}), its

envelope (black), 405-kyr LE extracted from the envelope of SE (black; 1/505 to 1/305 kyr^{-1}), 405-kyr LE (red; 1/505 to 1/305 kyr^{-1}), its envelope (black), 2.4-Myr GE extracted from the envelope of GE (black; 1/2900 to 1900 kyr^{-1}), 2.4-Myr GE (red; 1/2900 to 1900 kyr^{-1}), 173-kyr LO (red; 1/203 to 1/143 kyr^{-1}), its envelope (black), 1.2-Myr GO extracted from the envelope of LO (black; 1/1500 to 1/900 kyr^{-1}) and 1.2-Myr LO (red; 1/1500 to 1/900 kyr^{-1}), respectively. B) Average and evolutive wavelet periodogram. Target periodicities (kyr) indicated by dashed vertical lines for GE (2.4 Myr), GO (1.2 Myr), LE (405 kyr), LO (173 kyr) and SE (95 and 131 kyr, respectively). C) Assigned astrochronozones (De Vleeschouwer et al., 2017; Whalen et al., 2017). The cone of influence was removed from the wavelet periodogram for visual clarity (see Suppl. A). Note relative time based on floating astrochronology.

4.4.2. Sea level (Ti/Al, $\rho_{1,\ TOC}$ and $\rho_{1,\ Ti/Al}$)

Analogous to previous analyses, the imprint of Milankovitch cycles on proxies representing sea-level changes (Ti/Al, $\rho_{1,\ TOC}$ and $\rho_{1,\ Ti/Al}$) (Sageman et al., 2003; Li et al., 2018) were investigated and documented. Continuous wavelet transform analysis of Ti/Al reveals an apparent absence (or weak imprint) of LE. Even though increased power for SE appears to be present, this cannot be further tested due to the limited resolution of the dataset (i.e., absence of precession). In lack of unambiguous, conclusive evidence for LE modulating SE, these components are not interpreted to reflect eccentricity *per se* and are not further discussed. Conversely, a conspicuous ~2.4-Myr (g_4-g_3) cycle is recognized on Ti/Al (Fig. 7).

A moderate-to-weak imprint of LO can be observed (Fig. 7B), which is extracted using a Taner bandpass filter with a broad frequency window (1/203 to 1/143 kyr^{-1}) (Zeeden et al., 2019). As expected from frequency ratio calculations, roughly 7 LO cycles can be counted per GO cycle. Moreover, assessment of the envelope of LO and comparison of GO(i) and GO indicate excellent amplitude modulation patterns and phasing (Fig. 7A). Conversely, the g_4-g_3 cycle appears weak overall (Fig. 7C, D).

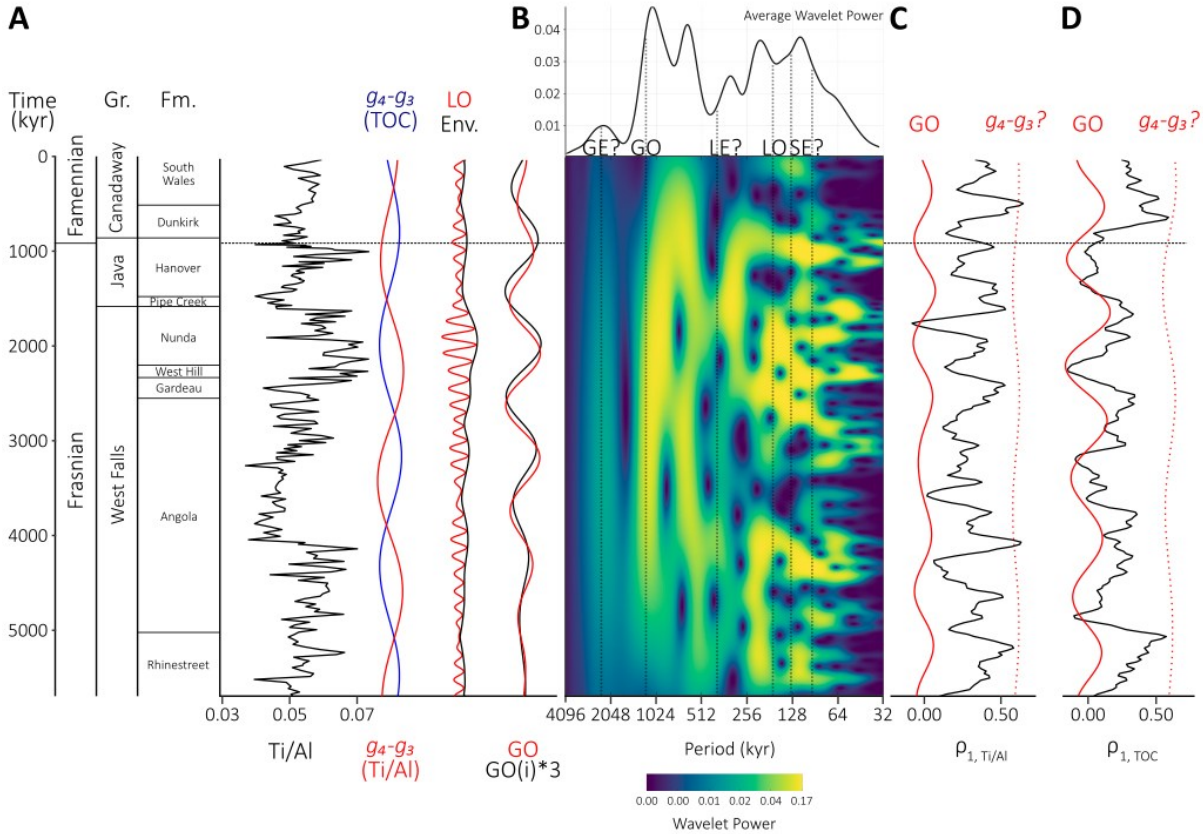

Fig. 7. Time-domain cyclostratigraphic analysis of sea-level change proxies. A) WVC stratigraphy: Stage, Group (Gr.) and Formation (Fm.), Ti/Al and bandpass filters corresponding to g_4-g_3 (Ti/Al, red; TOC GE, blue; 1/2900 to 1/1900 kyr^{-1}), 173-kyr LO (red; 1/203 to 1/143 kyr^{-1}), its envelope (black), 1.2-Myr GO extracted from the envelope of LO (black; 1/1500 to 1/900 kyr^{-1}) and 1.2-Myr GO (red; 1/1500 to 1/900 kyr^{-1}), respectively. Bandpass filter output corresponding to g_4-g_3 (TOC, Fig. 6) is added for comparison (blue). B) Average and evolutive wavelet periodogram of Ti/Al. Target periodicities (kyr) indicated by dashed vertical lines for GE (2.4 Myr), GO (1.2 Myr), LE (405 kyr), LO (173 kyr) and SE (95 and 131 kyr, respectively). C) $\rho_{1,\ Ti/Al}$ (black) and bandpass filter corresponding to 1.2-Myr GO (red) and g_4-g_3 (dotted red). D) $\rho_{1,\ TOC}$ (black) and bandpass filter corresponding to 1.2-Myr GO (red) and g_4-g_3 (dotted red). The cone of influence was removed from the wavelet periodogram for visual clarity (see Suppl. A). Note relative time based on floating astrochronology.

5. Discussion

5.1. WVC temporal framework and implications for the Kellwasser Crisis

The recognized, unambiguous imprint of Milankovitch cycles in multiple proxies enables the construction of a high-resolution (i.e., 0.1 Myr) floating astrochronology spanning 5.67 Myr for the WVC (Fig. S4). Because radiometric ages for the WVC are unavailable, the astrochronology is not anchored in this work. Temporal constraints can be provided on the duration of the WVC Rhinestreet, LKW, and UKW events and the Kellwasser Crisis interval (Table 1). Note that the duration of an Event is strongly tied to the criteria (e.g., (litho)stratigraphic unit, biostratigraphy, carbon isotope chemostratigraphy) used for its definition (Whalen et al., 2017; De Vleeschouwer et al., 2024). In the narrowest sense (i.e., (litho)stratigraphy), the LKW and UKW Event represent the black shales of the Pipe Creek Formation and the Point Gratiot Bed equivalent in the upper Hanover Formation, respectively, as expressed in the WVC strata (Fig. 2). Accordingly, the Kellwasser Crisis is estimated to encompass appr. 760 kyr. The durations of the LKW and UKW events are 84 kyr and 123 kyr, respectively. These estimated durations are close to those reported by Da Silva et al. (2020), 90 kyr and 130 kyr, respectively, and are in the order of magnitude of one short-eccentricity cycle. Moreover, based on lithostratigraphy, appr. 580 kyr separates the top of the Pipe Creek Formation (LKW) and the F-F boundary, perfectly consistent with the radiometric estimates provided by Percival et al. (2018). Finally, the duration of the Rhinestreet Event, as expressed in the WVC, is appr. 650 kyr according to the developed floating astrochronology. Given the absence of the lowermost Rhinestreet Formation in the WVC, this estimate represents a minimum constraint, suggesting that the actual duration could be longer (see also Kabanov et al., 2023).

Table 1. Astrochronologies for the Kellwasser Crisis. Table modified after De Vleeschouwer et al. (2024). All durations are based on $\delta^{13}C$ signatures.

Reference	Location	Kellwasser Crisis		LKW	UKW
		Onset-to-onset	Peak-to-peak		
Da Silva et al. (2020)	Germany	670 kyr	600-700 kyr	300 kyr	>400 kyr
De Vleeschouwer et al. (2017)	Global	600-700 kyr	800 kyr	100-300 kyr	>400 kyr
Ma et al. (2022)	South China	1300 kyr	1600 kyr	600 kyr	>405 kyr
Whalen et al. (2017)	Canada	500 kyr	650 kyr	200-250 kyr	>405 kyr

Wichern et al. (2024)	Germany	900 kyr	800 kyr	350 kyr	>405 kyr
This work	New York, USA	630 kyr	580 kyr	470 kyr	610 kyr

All temporal estimates provided here should be interpreted as ‘order-of-magnitude’ only as they were obtained by interpolating the 0.1-Myr-resolution floating astrochronology. Minor shifts in sedimentation rate (e.g., on precession-timescales) or small hiatuses that could not be captured may slightly impact the estimated durations. This is especially critical for the low resolution $\delta^{13}C_{org}$ chemostratigraphy.

Building on work by De Vleeschouwer et al. (2012; 2017) and Whalen et al. (2017), the WVC is put into the Frasnian astrochronologic framework (i.e., defining astrochronozones; Hilgen et al., 2020). According to their work, the Frasnian counts appr. 16.5 LE cycles (Fr-LEC). Thus, the last LE cycle is appointed Fr-LEC-16 (Fig. 6C). Similar to De Vleeschouwer et al. (2017), the WVC F-F boundary appears to occur slightly after the 405-kyr eccentricity minimum in Fa-LEC 1 (equivalent to Fr-LEC 17).

5.2. Geochemical proxy interpretation

The cyclostratigraphic framework of the WVC was established primarily using TOC as a proxy for preserved organic matter. This is complemented by additional insight into the Milankovitch imprint on sedimentation, captured through variations in Ti (coarse-grained detrital input), Ti/Al and, $\rho_{1,\,TOC}$ and $\rho_{1,\,Ti/Al}$ (sea-level variations) (Figs. 4, 6, 7, S2). While these proxies provide a robust foundation for constructing an astronomical age model, a broader paleoenvironmental and paleodepositional interpretation requires a more comprehensive assessment of the geochemical dataset.

More recently, somewhat contrasting views on establishing oxygenation levels, derived from paleoredox proxies, emerged; while Bennett and Canfield (2020) proposed (the use of) threshold values, Algeo and Liu (2020) caution against their use altogether. Following the recommendation by Algeo and Liu (2020), we refrain from applying fixed threshold values to redox-sensitive trace metal proxies, which should be established on formation-specific basis through internal cross-calibration of multiple redox proxies – something entirely out of scope for this work. Instead, qualitative paleoredox, -productivity and -hydrography conditions are discussed within a cyclostratigraphic framework to explore the influence of astronomical forcing on marine anoxia.

The clustering of TOC and typical redox-sensitive elements (Mo, Cu, Ni and V) along PC1 to PC3 (PCA; Fig. 3) is interpreted to primarily reflect a coupling between organic matter preservation and oxygen-depleted (suboxic to anoxic-euxinic) paleodepositional conditions (Tribovillard et al., 2006; Algeo and Liu, 2020). V undergoes a two-step reduction process that is strongly dependent on the intensity of reducing conditions (Tribovillard et al., 2006). Accordingly, V/Al is used to qualitatively distinguish between suboxic and anoxic-euxinic conditions.

In the absence of clear evidence for post-depositional diagenetic alteration, both Cu and Ni may serve as dual paleo-redox and -productivity proxies (Tribovillard et al., 2006; Tribovillard, 2021). Enrichment of Ni – particularly when associated with other paleoredox indicators such as V and Mo, and elevated TOC-values – suggests a coupling between enhanced paleoproductivity and anoxic conditions (Tribovillard et al., 2006, Tribovillard, 2021). Accordingly, an increase in Ni_{EF} is interpreted as indicative of elevated paleoproductivity and, when accompanied by enrichment in other redox-sensitive elements, a decline in bottom-water oxygenation. Due to its moderate-to-weak loading in the PC1-PC2 space (Fig. 3), Cu is not further considered within a cyclostratigraphic context.

Sedimentary Mo is typically enriched in organic-rich marine facies deposited under anoxic conditions and is widely used as a proxy for benthic redox potential, particularly in association with other paleoredox proxies such as V (Algeo and Lyons, 2006; Tribovillard et al., 2006). In restricted marine environments, Mo burial generally peaks in weakly sulfidic paleoenvironments and tends to be lower under strongly sulfidic conditions (see Algeo and Lyons, 2006). Thus, lowered Mo-values during an anoxic interval may signal more intensely reducing (sulfidic) conditions. However, Mo is highly sensitive to reservoir effects in anoxic silled basins (Algeo and Lyons, 2006) – conditions that likely prevailed intermittently in the Late Devonian Appalachian Basin (Algeo et al., 2025). Consequently, the Mo/Al ratio is not only reflective of redox conditions but is also linked to hydrographic restriction of the deep-water mass, making it an amalgamated signal. Short-scale punctuated increases in Mo/Al are interpreted as enrichment due to marine anoxia, whereas long-term (secular) Mo/Al changes are indicative of variations in water-mass restriction, serving as a paleohydrography proxy (Algeo and Lyons, 2006). This interpretation is complemented by Mo/TOC, which decreases under increasing restriction (Algeo and Lyons, 2006). Specifically, secular increases in Mo/Al and Mo/TOC suggest reduced restriction (e.g., transgression (Ti/Al) in the middle Angola Fm. renewing the Mo-budget, causing highest Mo/Al and Mo/TOC spikes; Fig. 8), while declines imply enhanced restriction. The latter can be observed on the largest scale as relative sea-level decreases from the Rhinestreet Fm. onwards (Sageman et al., 2003), leading to decreasing Mo/Al up to the base of the Pipe Creek Fm. (Fig. 8). In all cases, normalization to Al did not introduce spurious correlations (Van der Weijden, 2002).

The recycling of phosphorus (P), a limiting nutrient for primary production, has been thoroughly highlighted for the Kellwasser Crisis (WVC) by Murphy et al. (2000) and Percival et al. (2020). Indeed, the clustering of P and Mn, opposing the TOC-cluster (Fig. 3), indicates that the paleoredox conditions exerted dominant control on P availability (Algeo and Scheckler, 1998; Murphy et al., 2000; Percival et al., 2020; Sageman et al., 2003). Specifically, the anti-phasing of TOC and P peaks strongly suggests a coupling between bottom-water oxygenation, benthic phosphorus retention, and marine primary productivity (Van Cappellen and Ingall, 1994), and is interpreted here as a signal of marine anoxia.

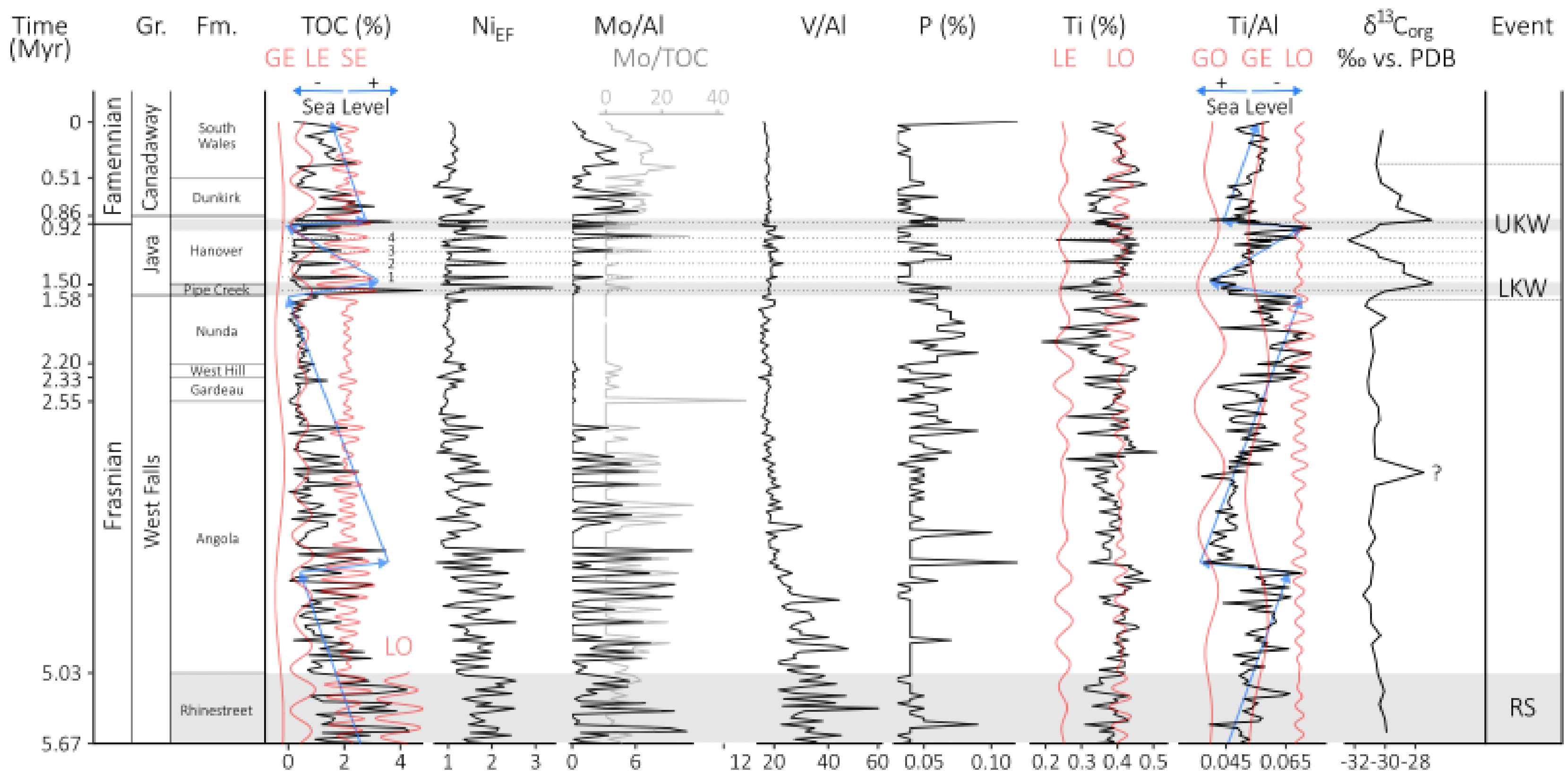

Fig. 8. WVC geochemical profiles in relative time. From left to right; WVC stratigraphy: Stage, Group (Gr.) and Formation (Fm.); TOC (%) incl. ~100-kyr SE, 173-kyr LO (RS), 405-kyr LE and 2.4-Myr GE bandpass filter output; Ni$_{EF}$; Mo/Al; Mo/TOC; V/Al; P(%); Ti (%) incl. 173-kyr LO and 405-kyr LE bandpass filter output; Ti/Al incl. 173-kyr LO, 1.2-Myr GO and 2.4-Myr GE bandpass filter output, blue arrows indicate major transgression/regression trends, based on Ti/Al (Sageman et al., 2003); $\delta^{13}C_{org}$; Anoxic event intervals of the Rhinestreet (RS), Lower Kellwasser (LKW) and Upper Kellwasser (UKW) are indicated in light gray; dotted lines in the Kellwasser Crisis interval indicate maxima in ~100-kyr SE. Dashed gray lines indicate lower and upper boundaries of the Kellwasser Crisis based on CIE trends. See Figs. 6, 7 and Suppl. A for details on used bandpass filter windows. Note relative time based on floating astrochronology.

5.3. *Eccentricity pacing of marine anoxia*

The strong imprint of eccentricity on TOC (Fig. 6), redox conditions (Ni_{EF}, Mo/Al, V/Al; Fig. 8; Fig. S5), and on variations in coarse-grained detrital input (Ti; Figs. 8, S2) demonstrates a significant influence of astronomical forcing on sedimentary and organic matter deposition in the Late Devonian Appalachian Basin. Peak OM accumulation and preservation (TOC) coincides with SE maxima throughout the record, most strikingly in the Kellwasser Crisis interval, but also in the Rhinestreet Formation, and is strongly indicative of eccentricity pacing of marine oxygen depletion. Conversely, an increase in coarse-grained material (Ti; Calvert and Pedersen, 2007; Croudace and Rothwell, 2015) during eccentricity minima is interpreted to reflect a relative increase in mechanical erosion, suggesting increased aridity and a relative weakening of monsoonal activity (e.g., Wichern et al., 2024). Under such a scenario, fewer nutrients would reach the basin, leading to reduced primary productivity (Ni_{EF}, Fig. 8; Jaminski et al., 1998; Sageman et al., 2003; Liu et al., 2019).

Given the quasi-absence of eccentricity in the power spectrum of insolation (Berger, 1988), its strong imprint on OM accumulation and preservation suggests a non-linear mechanism, such as amplification of positive (or negative) extremes, which effectively demodulate the forcing (Hays et al., 1976; Wigley, 1976). During eccentricity maxima, precession modulation is strongest, amplifying climatic extremes. Because precession commonly drives monsoonal variability in warm climates such as the Devonian (De Vleeschouwer et al., 2014; Wichern et al., 2024), maximum eccentricity configuration may enhance nutrient influx and cause eutrophication (De Vleeschouwer et al., 2024), leading to black shale deposition.

For the Late Devonian, previous work (De Vleeschouwer et al., 2017; Whalen et al., 2017; Da Silva et al., 2020; Ma et al., 2022; Wichern et al., 2024) already documented the relationship between Milankovitch cycles and the (Upper) Kellwasser Event(s), highlighting the contribution of astronomical forcing as (a part of) a pacing mechanism of anoxic events. Most recently, Wichern et al. (2024) demonstrated precession-sensitive monsoonal climate during the Kellwasser Crisis interval in Germany. However, direct evidence linking marine anoxia (i.e., paleoredox conditions and OM enrichment) to precession-controlled monsoonal climate is still lacking. To further investigate whether such mechanisms could explain the strong imprint of eccentricity (modulating precession), new high-resolution geochemical data of Kellwasser Crisis sections is required. In addition, (geo)physical climate modelling may equally play a crucial role in advancing of our understanding the role of astronomical forcing on marine anoxia. Whilst the aforementioned studies primarily focused on the relationship between Milankovitch cycle extrema, event timing and carbon isotopic shifts, no explicit evidence was brought forth documenting the astronomical pacing of marine anoxia (De Vleeschouwer et al., 2017; Whalen et al., 2017; Da Silva et al., 2020; Ma et al., 2022; Wichern et al., 2024). This study demonstrates, for the first time, that short-eccentricity cycle maxima controlled the pacing of OM enrichment and paleoredox conditions during the Kellwasser Crisis, highlighting astronomical forcing as a key driver of marine anoxia in the Frasnian Appalachian Basin.

Eccentricity control on OM is consistent with a climate-driven mechanism for anoxia development, likely involving changes in weathering profiles, nutrient runoff and/or productivity (Carmichael et al., 2019; Percival et al., 2019; Algeo and Shen, 2024; De Vleeschouwer et al., 2024; Fig. 8). Even though a volcanic trigger (or contribution) cannot be excluded, cyclic variations in weathering, productivity, and carbon burial, as well as an increase in $\delta^{13}C_{org}$ are consistent with an astronomically-forced, productivity-driven biocrisis (Carmichael et al., 2019; Algeo and Shen, 2024; De Vleeschouwer et al., 2024). Bio-evolutionary events driving land-plant colonization, weathering (Algeo and Scheckler, 1998), and CO_2-drawdown (Algeo et al., 2001) could at least have created environmental stress bringing the Earth system close to the tipping point for biocrisis (Smart et al., 2023; Algeo and Shen, 2024). Whereas volcanism may have further contributed to additional environmental stress (e.g., Pisarzowska and Racki, 2020), for the Appalachian Basin, it does not appear to have been the (sole) trigger mechanism. The consistent ~100-kyr pacing of pulses of anoxia during the Kellwasser Crisis interval strongly suggests that astronomically forced insolation change may have ultimately triggered and paced the onset of anoxia.

5.4. Obliquity pacing of sea-level variations

In contrast to the dominant control of eccentricity on OM, coarse-grained detrital input and redox conditions, a strong imprint of obliquity has been recovered from proxies for sea-level change (Ti/Al, $\rho_{1,\,TOC}$ and $\rho_{1,\,Ti/Al}$; Fig. 7), indicating strong astronomical control on third-order sea-level fluctuations through 1.2-Myr GO cyclicity. The GO cycles recovered from $\rho_{1,\,TOC}$ and $\rho_{1,\,Ti/Al}$ are anti-phased to the 1.2-Myr GO cycle extracted from Ti/Al which is expected as minima in Ti/Al indicate maxima in relative sea level, while maxima in ρ_1 indicate minima in sedimentary noise and, thus, maxima in relative sea level (Li et al., 2018). The recovered LO imprint from Ti/Al provides additional insight into fourth-order cycles despite its moderate-to-weak amplitude, which is primarily interpreted to reflect a decreased sensitivity to obliquity changes on the 173-kyr timescale. Fluctuation of LO-associated power may also be due to the overall weaker amplitude of the s_3-s_6 term (Laskar, 2020) and instability beyond 50 Ma (Zeebe and Lantink, 2024).

Recovery of a ~2.4-Myr cycle imprint on Ti/Al variations (interpreted to reflect sea-level changes), is surprising at first glance. Indeed, the ~2.4-Myr g_4-g_3 cycle is classically associated with the modulation of eccentricity terms, while the Ti/Al signal displays an unclear imprint of SE and LE (Fig. 7). Both SE and LE are expected to be stronger in amplitude than GE (Laskar, 2020) and were found to dominate TOC (Fig. 6). Instead, this 2.4-Myr cycle is interpreted to originate from a strong obliquity imprint. In fact, the g_4-g_3 term influences not only the modulation of precession (and eccentricity) but also the modulation of obliquity (i.e., the envelope of obliquity contains the 2.4-Myr g_4-g_3 cycle; see figure. 4.15 in Laskar, 2020 and table 4 and figure 6 in Zeebe and Kocken, 2025). Recovery of the anti-phasing g_4-g_3 cycles in eccentricity and obliquity hints at the s_4-s_3 = 2(g_4-g_3) resonance being active (e.g., Laskar, 2020) during the Late Devonian. This also indicates that, also on a Myr-timescale, baseline TOC increases as relative sea-level increases (and Ti/Al decreases). Such a scenario is consistent with interpreted deepening and black shale deposition (e.g., Sageman et al., 2003). In addition, the consistent anti-phasing between the g_4-g_3 (TOC) and g_4-g_3 (Ti/Al) (Fig. 7) further validates the proposed astronomical age model.

Typically, two dominant mechanisms are invoked to explain sea-level fluctuations within a cyclostratigraphic framework, depending on the prevailing climatic regime (Li et al., 2018). During cooler intervals (e.g., the Quaternary) with significant ice sheets, sea level is primarily regulated through 'glacio-eustasy' (continental volume ice changes) (Lourens and Hilgen, 1997). In contrast, during globally warmer intervals without major ice sheets, sea level is largely influenced by 'aquifer-eustasy' or 'limno-eustasy' (variations in groundwater and lake volume) and thermal expansion (Miller et al., 2005; Li et al., 2018; see also references in Kabanov et al., 2023). Higher sea levels can be interpreted differently depending on the governing mechanism. Under a 'limno-eustasy' eustatic regime, higher sea level would correspond to lower obliquity, as reduced seasonality causes the lake and groundwater system to release water in the ocean (Li et al., 2018). Conversely in a 'glacio-eustatic' regime, higher sea level would correspond to higher obliquity, which enhances summer melting and reduces ice volume (e.g., Lourens and Hilgen, 1997). During a greenhouse period such as the Late Devonian, limno-eustasy represents a more probable dominant mechanism (with a contribution by thermal expansion) controlling minor sea-level variations (Kabanov et al., 2023).

The observed anti-phasing between the g_4-g_3 extracted from TOC and the g_4-g_3 extracted from Ti/Al (Fig. 7) is leveraged to shed light on which mechanism predominantly controls sea-level fluctuations. Assessment of an astronomical solution (La04, from 0 to 20 Ma during which the s_4-s_3 = 2(g_4-g_3) resonance is active; Laskar et al., 2004) illustrates that anti-phasing of the g_4-g_3 cycle can be expected depending on whether it is extracted from eccentricity or from the envelope of obliquity (Fig. 9) – coherent with what can be observed for the g_4-g_3 cycle extracted from TOC and Ti/Al, respectively (Fig. 7). Analogous to such a scenario, for the WVC, high eccentricity reflects high TOC and, accordingly, high obliquity reflects high Ti/Al (or low sea-level). This scenario aligns with 'limno-eustasy', most clearly paced by obliquity at 1.2-Myr and 2.4-Myr timescales. Nevertheless, glacio-eustatic sea-level variations operating on different timescales – such as those potentially linked to the cooling pulses associated with the Kellwasser events (Joachimski and Buggisch, 2002; Huang et al., 2018; Algeo and Shen, 2024) – cannot be entirely ruled out (Algeo et al., 2025).

Although uncertainty regarding the amplitude of sea-level changes during the Devonian remains (Kabanov et al., 2023), even smaller (~5 m) amplitude-variations of third-order cycles could have played a major role in the deposition of Devonian black shales in the semi-restricted Appalachian Basin (Algeo et al., 2025). This is exemplified most clearly by the coinciding transgression and OM enrichment during the LKW and UKW and relative highstand during the deposition of the black shales of the Rhinestreet Formation (Fig. 8). As such, changes in eustatic sea-level are unequivocally associated with anoxic (extinction) events in the Appalachian Basin. This provides strong evidence that obliquity played a role in Frasnian marine anoxia, either through the upwelling of nutrients or the intrusion of anoxic water-masses, particularly during the Rhinestreet, LKW, and UKW events.

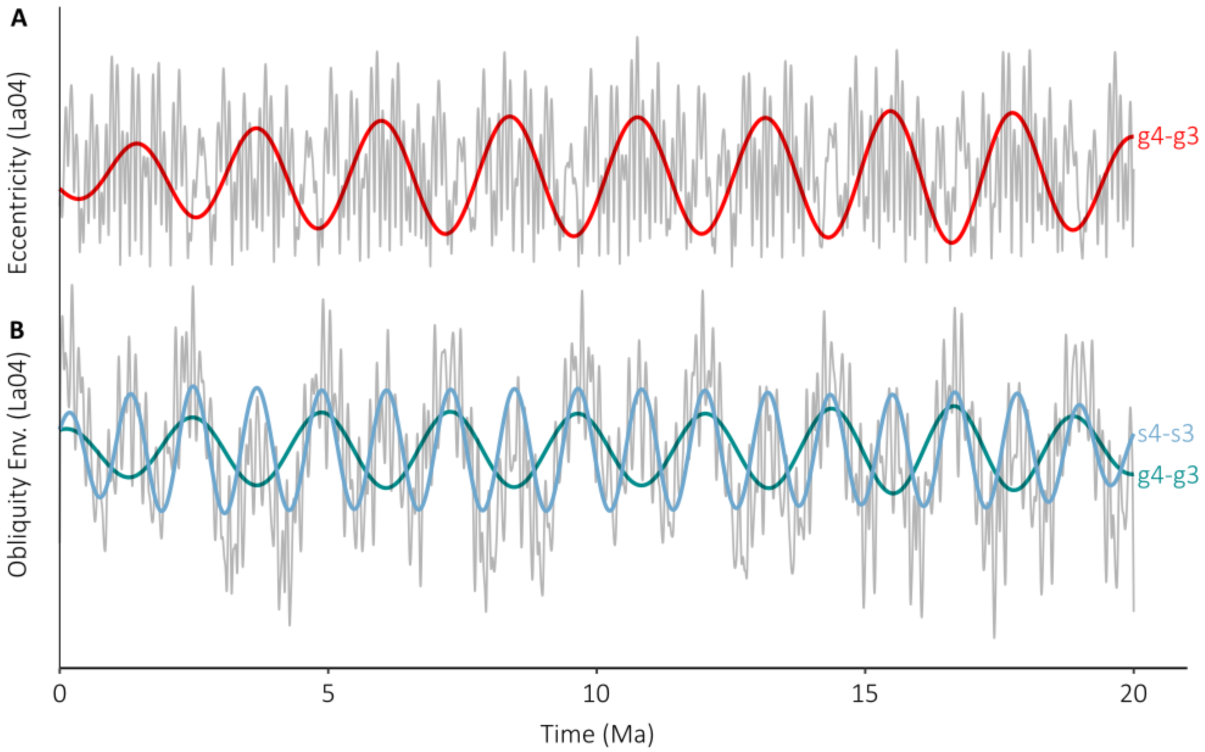

Fig. 9. Eccentricity and obliquity for the last 20 Myr (La04). A) La04 solution for eccentricity (0-20 Ma; Laskar et al., 2004) (gray) and extracted g_4-g_3 cycle (red). B) Envelope of the La04 solution for obliquity (0-20 Ma; Laskar et al., 2004) obtained via a Hilbert transform (gray), subsequently extracted g_4-g_3 (cyan) and s_4-s_3 (blue).

5.5. Controls on the succession of events through the middle and late Frasnian

5.5.1. Rhinestreet Event

The global Rhinestreet (RS) anoxic event (Becker et al., 2020) represents a period of prolonged, significant marine anoxia, as is exemplified by its large thickness and protracted duration (estimated 650 kyr in this work; compared to > 600 kyr in Becker et al., 2020; > 1 Myr in Kabanov et al., 2023). The black shales of the Rhinestreet Formation are interpreted to have recorded progradational/retrogradational cycles (Lash and Blood, 2006). Flexural adjustments, subsidence, and rebound resulting from the ongoing Acadian Orogeny would have lesser influence (especially during mid to late portions of tectophases) (Ver Straeten, 2009; 2010; 2023), superimposed onto astronomically forced eustatic sea-level variations. In the WVC, the Rhinestreet Event is characterized by high TOC values (up to 4%), enrichment of paleoredox elements (e.g., Ni_{EF}, Mo/Al, V/Al; see Fig. 8) indicating increased paleoproductivity and oscillating anoxic to euxinic conditions. Elevated Mo/Al and Mo/TOC values in the Rhinestreet (and lower Angola) Formation (Fig. 8), indicate minimal restriction in the Appalachian Basin (cf. Algeo and Lyons, 2006), an interpretation that is consistent with high eustatic sea-levels associated with the RS Event (Sageman et al., 2003; Becker et al., 2020).

Here, the Rhinestreet Formation stands apart from the overlying strata by an equally strong eccentricity and 173-kyr obliquity imprint on OM accumulation and preservation (Fig. 8). TOC peaks during ~100-kyr eccentricity maxima (modulated by LE), indicating climatically-induced forcing of marine anoxia. Yet, the relative amplitude of peaks in TOC appears dictated by 173-kyr variations (see Fig. 8), suggesting a strong contribution to anoxia development by obliquity. Based on the correlation of known global marine transgressions and co-eval gray/black shale intervals, Lash and Blood (2006) suggested that (fourth-order) eustatic oscillations played a role in the deposition of black shales, which would be consistent with 173-kyr obliquity forcing (considering the extensive role of obliquity forcing on sea level). Such a pronounced obliquity imprint may be due to the highest relative sea level in the Appalachian Basin during the deposition of the Rhinestreet Formation (Mo/Al, Mo/TOC Fig. 8; see also Sageman et al., 2003; Ver Straeten et al., 2011).

5.5.2. Kellwasser Crisis

In the Appalachian Basin, the pre-Kellwasser interval is characterized by the sandstones of the Nunda Formation, predominantly deposited during periods of strong obliquity modulation (maxima in s_4-s_3 and g_4-g_3 for obliquity, akin to Fig. 9) and associated lowstand conditions (Figs. 8, 10). Note that maximal g_4-g_3 for obliquity corresponds to minimal g_4-g_3 for eccentricity (Fig. 9). Consequently, the deposition of this interval is interpreted to have occurred during a 2.4-Myr eccentricity cycle minimum (i.e., node), suggesting a period characterized by the avoidance of climatic extremes and potentially a weakened monsoonal climate (Wichern et al., 2024). Furthermore, low levels of TOC and paleoredox proxies (Ni_{EF}, Mo/Al and V/Al, Fig. 8) indicate well-oxygenated bottom waters, while high Ti indicates increased coarse-grained detrital input (Fig. 8). As eccentricity increased and strong obliquity modulation diminished, sandstone deposition ceased in the run-up to the LKW Event.

The LKW Event (Pipe Creek Formation) occurs after a node in eccentricity (Nunda Formation), strongly reminiscent of the UKW 'nutrient-gun' hypothesis (De Vleeschouwer et al., 2024), and culminates appr. 200 kyr later (half LE cycle). The onset of the LKW Event appears rapid (≤100 kyr timescales), OM accumulation and preservation is paced by eccentricity, and the associated transgression appears paced by 173-kyr obliquity. However, the amplitude of the excursion in Ti/Al does not reflect the amplitude in 173-kyr obliquity, most probably indicating that processes driving flooding on yet shorter timescales should be investigated. Peak TOC values are recorded in the subsequent 173-kyr LO and 1.2-Myr GO minima (i.e., maximum flooding) and coincide with SE and LE maxima (Figs. 8, 10D). The low-obliquity, high-eccentricity configuration would lead to relatively elevated sea levels and increased clay and nutrient inputs (decreased Ti), respectively (Fig. 10D). This would consequently amplify eutrophication through increased nutrient influx and productivity (see Ni_{EF}, Fig. 8) and upwelling of either nutrient-rich or oxygen-depleted bottom-waters (Carmichael et al., 2019) through ocean circulation invigoration (Algeo and Shen, 2024). Although anoxic (*sensu stricto)* conditions appear to have been mostly absent (based on

Mo/Al, V/Al; Fig. 8) in this interval of the WVC, productivity and OM burial were maximal, displaying highest TOC and Ni_{EF} values for the entire record. The anti-phased response of P relative to TOC may indicate P-recycling under reducing conditions (Murphy et al., 2000; Percival et al., 2020), contributing to sustained oxygen depletion (increased Mo/Al and V/Al) and prolonged black shale deposition (TOC) during the associated transgression (thereby potentially renewing the Mo-budget) (Fig. 8).

The inter-Kellwasser interval (lower to middle Hanover Formation) displays strong ~100-kyr short-eccentricity pacing of deoxygenation (Ni_{EF}, Mo/Al, V/Al; Fig. 8) and OM preservation (TOC spikes 1 to 4 on Fig. 8). This contrasts with other sections (e.g., Kowala, Poland) that display a period of non-response to orbital forcing in this interval (De Vleeschouwer et al., 2013) and was, based on increased obliquity power, interpreted to represent a node in eccentricity by De Vleeschouwer et al. (2017) and Da Silva et al. (2020). Such contrast may, in part, be attributed to the large variety in how the Kellwasser Crisis is expressed (Carmichael et al., 2019) and may thus reflect regional influences. This may also reflect the spatially heterogeneous transfer of astronomical forcing into the ocean's biogeochemical response (Gérard et al., 2025), with local circulation exerting a key control on the distribution of these patterns.

Nevertheless, in the Appalachian Basin, this interval experiences oscillating dysoxic to anoxic conditions and increased paleoproductivity (Ni_{EF}). Spikes in Mo/Al are interpreted to represent increasing dysoxic to anoxic conditions and Mo-burial (Algeo and Lyons, 2006). Renewal of the Mo budget is attributed to the preceding LKW transgression. Yet, it should be mentioned that a steady regression coincides with this interval (Ti/Al; Fig. 8). Most striking is that TOC spike 4 (Fig. 8) appears protracted compared to previous pulses and paleoredox proxies point towards anoxic to slightly euxinic conditions (Fig. 8), indicating strong paleoenvironmental stress on the biosphere. This spike (4) coincides with a 173-kyr minimum, which may also explain elevated Mo/Al and Mo/TOC (i.e., reduced restriction; Fig. 8) and why it appears more protracted and more anoxic to euxinic. Similar to the LKW Event, P appears anti-phased to TOC, indicating that P-recycling is possibly contributing to sustained oxygen depletion and recurring black shale deposition.

The UKW represents the major, 1^{st}-order extinction pulse at the F-F boundary (Raup and Sepkoski, 1982; Brett et al., 2020; Algeo and Shen, 2024) in the upper Hanover Formation (Over, 1997). In the WVC, it is characterized by one minor TOC spike, followed by a second major peak in TOC marking the culmination of the UKW OM burial during a ~100-kyr eccentricity maximum and during the decreasing limb of 173-kyr obliquity (i.e., transgression) (Fig. 8; n.b. see Algeo et al., 2025, for higher-resolution chemostratigraphic records of this interval). Although coinciding TOC, Ni_{EF} and Mo/Al spikes (Fig. 8) indicate oxygen depletion, V/Al remains relatively low, suggesting that dysoxic conditions prevailed. Increases in Ni_{EF} and Mo/Al hence may have been associated with increased paleoproductivity and decreased restriction as a result of the UKW transgression (Mo/TOC, Ti/Al; Fig. 8). The amount of time separating these peaks appears considerably shorter than 100 kyr, strongly suggesting that the first minor TOC peak is paced by short obliquity or precession (note that this part of the dataset has higher resolution, allowing for such a statement). In contrast to the LKW Event, the UKW Event peak TOC values occur after a LE minimum (Fig. 8). Such a scenario similarly reminds of the 'nutrient-gun' hypothesis (De Vleeschouwer et al., 2024), albeit following a minimum in LE instead of GE. The final peak in TOC at the F-F boundary marks the culmination of a series of ~100-kyr SE-paced anoxia pulses, probably causing the strongest environmental stress. What further differentiates the UKW from the prior anoxia pulses and OM burial episodes is the orbital configuration associated with the rapid transgression; relative sea level gradually declined in the inter-KW interval, culminating during a maximum in 173-kyr and 1.2-Myr obliquity near the F-F boundary (s_4-s_3 and s_3-s_6, respectively) (Fig. 8). This is in stark contrast with the minimum in 1.2-Myr obliquity (i.e., higher relative sea level) associated with the LKW Event through the WVC.

The post-Kellwasser interval is represented by the lower Dunkirk Formation (earliest Famennian) in the Appalachian Basin. Even though it still exhibits considerable OM enrichment (TOC), paleoproductivity (Ni_{EF}) further decreases (Fig. 8). A relative increase in Mo/Al is interpreted to result primarily from a rising relative sea level on 1.2-Myr timescales (GO, Ti/Al; Fig. 8)., renewing the Mo-budget. As baseline relative sea-level would continue to decrease (on > 1.2-Myr timescales, attributed mostly to progradation of synorogenic sediments of the Catskill Delta complex eroded from the Acadian Orogen (Ver Straeten, 2009; 2010; Smith and Jacobi, 2023), it becomes apparent that the influence of obliquity on OM enrichment and black shale deposition diminishes. OM burial appears to be paced dominantly by both SE and LE, which is exemplified by TOC peaks coinciding with ~100-kyr SE maxima (and lower TOC-values during the GO maximum).

5.6. A new cyclostratigraphic model for the Kellwasser Crisis

An interplay between eccentricity and obliquity forcing (over a range of timescales) dominated the Frasnian Appalachian Basin and, more specifically, the Kellwasser Crisis interval. Even though 1.2-Myr obliquity forcing appears to dominate the WVC record, both LKW and UKW are clearly associated with shorter-term (173-kyr or short obliquity?) eustatic sea-level variations (Figs. 7, 8). Short (~100-kyr) eccentricity maxima pace TOC throughout the record, most strikingly in the Kellwasser Crisis interval (Figs. 6, 8). These observations provide the foundation for formalizing a new model for astronomical forcing during the Kellwasser Crisis in restricted basins such as the Appalachian Basin. Here, a low-eccentricity configuration at ~100 kyr is associated with increased coarse-grained detrital influx (Ti), potentially indicating a weakened monsoonal system and lower nutrient-availability (Fig. 10A, B). Even though 173-kyr obliquity forcing (also affecting seasonal contrast) may modulate the amount of clay and nutrient influx (cf. Jaminski et al., 1998; Liu et al., 2019), the low-eccentricity scenario appears not conducive for anoxia and black shale deposition – regardless of relative sea-level changes.

Conversely, a high-eccentricity configuration at ~100 kyr would amplify seasonality, by intensifying monsoonal systems on precession timescales (De Vleeschouwer et al., 2014; Wichern et al., 2024), and intensify nutrient runoff, causing eutrophication and anoxia development (Fig. 10C, D), as suggested in the astronomical scenarios by Ma et al. (2022) and De Vleeschouwer et al. (2024). Clay and nutrient input would be maximized under a high-eccentricity, high-obliquity configuration (i.e., strongest seasonality; similar to the model proposed by Ma et al., 2022 – yet, on shorter timescales in this scenario). Even though under a high-eccentricity, low-obliquity orbital configuration (Fig. 10D), clay and nutrient influx would no longer be maximal, the oceanic invigoration and co-occurring transgression would enforce oxygen depletion and reducing conditions (Carmichael et al., 2019; Kabanov et al., 2023, Algeo and Shen, 2024), maximizing black shale deposition. Even though OM enrichment appears to occur regardless of relative sea-level, obliquity-forced transgression (Fig. 10D) appears to exacerbate anoxia and trigger maximal stress on the biosphere (i.e., mass extinction/depletion; Carmichael et al., 2019; Brett et al., 2020). Yet, it remains unclear whether the transgressions associated with the deposition of black shales during the LKW and UKW represent a primary or secondary contribution. Resolving short obliquity would be required to shed light on this by investigating the succession of events on even shorter (10^4-yr) timescales. Regardless of whether the associated transgressions were entirely astronomically forced, their potential for contributing to anoxia (Carmichael et al., 2019; Kabanov et al., 2023) remains unchanged. Phosphorus influx and recycling under reducing conditions (Percival et al., 2019, 2020) may provide a pathway to sustaining eutrophication. However, this mechanism remains debated (Reershemius and Planavsky, 2021) and recent simulations (Gérard et al., in review) suggest that the variations of phosphate, induced by astronomical forcing, may be either too gradual or too limited in amplitude to trigger or maintain an anoxic state over extend timescales. Nevertheless, coinciding decreases in P and increases in TOC, Ni_{EF}, Mo/Al and V/Al underscore transient reducing paleoenvironmental conditions (Van Cappellen and Ingall, 1994; Tribovillard et al., 2006), especially in the Kellwasser Crisis interval.

Even though existing cyclostratigraphic interpretations (‘eccentricity-minimum’ hypothesis; De Vleeschouwer et al., 2017; 2024; Da Silva et al., 2020; Wichern et al., 2024 and ‘maximum obliquity and eccentricity’ hypothesis; Ma et al., 2022) differ to some extent, they both rely on climatically-induced anoxia, induced by increased nutrient-runoff causing eutrophication (Ma et al., 2022; De Vleeschouwer et al., 2024). Interestingly, despite the often-clear association between transgression and the Kellwasser events, as well as the observed Myr-obliquity imprint (see Ma et al., 2022), the role of eustatic sea-level variations in contributing to anoxia has not yet been considered within an astronomical framework. Here, the interplay between eccentricity- and obliquity-forced anoxia is recognized. In accordance with existing models by Da Silva et al. (2020), De Vleeschouwer et al. (2017; 2024) Ma et al. (2022) and Wichern et al. (2024), deposition and preservation of anoxic facies (e.g., black shales) were maximal during periods of maximum (short) eccentricity (i.e., maximal modulation of precession). Such a scenario is consistent with climate-driven anoxia (Jaminski et al., 1998; Liu et al., 2019; De Vleeschouwer et al., 2024). In complement, obliquity-forced sea-level variations equally contributed to marine anoxia. Whilst influx of nutrient-rich bottom waters could contribute to eutrophication, recent work by Gérard et al. (2025) suggests that, on the other hand, obliquity-forced ocean circulation and oxygen solubility changes may have caused upwelling of anoxic bottom waters.

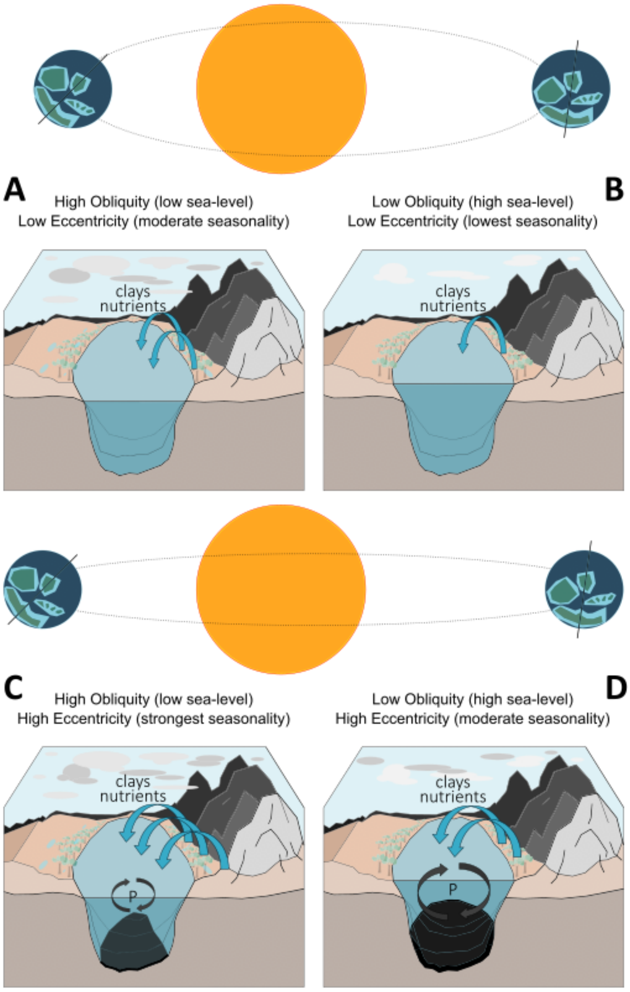

Fig. 10. Cyclostratigraphic model for the Kellwasser Crisis in a restricted (Appalachian) basin. A) High-obliquity, low-eccentricity orbital configuration corresponding to relatively low eustatic sea level and moderate seasonality resulting in moderately low influx of clays and nutrients from land. B) Low-obliquity, low-eccentricity orbital configuration corresponding to relatively high eustatic sea level and low seasonality resulting in a low influx of clays and nutrients from land. C) High-obliquity, high-eccentricity orbital configuration corresponding to relatively low eustatic sea level and strongest seasonality, resulting in the largest influx of clays and nutrients from land, increased P-recycling under oxygen-depleted conditions and OM deposition. D) Low-obliquity, high-eccentricity orbital configuration corresponding to relatively high eustatic sea level and strong seasonality, resulting in large influx of clays and nutrients from land, maximally increased P-recycling under oxygen-depleted conditions and maximal OM deposition. Blue arrows indicate influx of clays and nutrients (based on lower coarse-grained input; Ti), black arrows indicate phosphorus recycling and, hence, benthic anoxic (reducing) conditions.

Lastly, it should be mentioned that the proposed orbital configuration of maximal ~100-kyr eccentricity and obliquity-driven transgression (Fig. 10D) associated with the LKW and UKW events is not unique. Such an astronomical configuration would have occurred frequently, whereas marine anoxia appears to have been less common, indicating that other factors should be considered to explain marine anoxia development.

Even though many trigger mechanisms may be invoked that could cause regional-to-global climate perturbations and make the Earth system prone to anoxia, evidence from the WVC record hints, again, at a combined effect of seasonal contrast and sea-level variations. During the deposition of the pre-KW Crisis sandstones of the Nunda Formation, lowstand (1.2-Myr GO maximum as well as decreased subsidence; Lash and Blood, 2006: Smith and Jacobi, 2023) coincided with a node in eccentricity, during which there is a strong avoidance of seasonal contrast during a period of 405 kyr (De Vleeschouwer et al., 2024). Potentially, the termination of such long-term climatic stability during the deposition of the upper Nunda Formation may have induced rapid bio-evolutionary events (i.e., 'strong version' of the land-plant weathering hypothesis, Algeo et al., 1995; Algeo and Shen, 2024). This way, the Earth system may have been sufficiently stressed and brought close to the tipping point towards marine anoxia and extinction (Algeo and Shen, 2024).

6. Conclusions

A strong astronomical imprint on the WVC strata is recognized in multiple geochemical proxies. Short-eccentricity maxima paced enrichment and preservation of OM (TOC), oxygen depletion suggesting transient anoxia (Ni_{EF}, Mo/Al, V/Al) and influx of coarse-grained detrital material (Ti) indicating reduced monsoonal activity. A strong imprint of obliquity on Ti/Al, $\rho_{1, TOC}$ and $\rho_{1, Ti/Al}$ – most clearly paced by 1.2-Myr and 2.4-Myr cycles – strongly highlights astronomical control on eustatic sea-level fluctuations, predominantly through limno-eustasy. Coinciding orbitally-forced transgression and pacing of oxygen depletion implies strong orbital control on the Kellwasser Crisis interval and, most strikingly, on the LKW and UKW events. In the Appalachian Basin, the Kellwasser events are separated by four sharp peaks in TOC, paced by short eccentricity maxima. OM enrichment during the Rhinestreet Event appears paced by both 173-kyr obliquity and short- and long-eccentricity cycles, interpreted to be mediated through relative eustatic highstand.

Based on the recovered imprint of Milankovitch cycles on the WVC strata, a new model for astronomical control on the Kellwasser events in the Appalachian Basin is proposed. It reconciles existing cyclostratigraphic models for the Kellwasser Crisis (Da Silva et al., 2020; De Vleeschouwer et al., 2017; 2024; Ma et al., 2022; Wichern et al., 2024) in terms of causal mechanisms, with high eccentricity driving increased nutrient runoff, eutrophication and marine anoxia as well as the influence of obliquity on eustatic sea-level variations. Yet, it provides a novel, more detailed synthesis of the orbital configuration commonalities of the LKW and UKW Event; an interplay of obliquity-forced transgression and eccentricity-forced increased monsoonal activity. Accordingly, an interplay of eccentricity- and obliquity-forced mechanisms for anoxia development have governed OM accumulation and preservation in the Appalachian Basin. However, since the orbital configurations associated with the Kellwasser events are not unique, it is highly probable that astronomical forcing was not the sole causal mechanism. The LKW Event appears to have occurred after a 405-kyr-period of prolonged avoidance of seasonal extrema (i.e., a node in 2.4-Myr grand eccentricity) and marks the onset of the Crisis interval. The UKW Event appears to have occurred on the rising limb of short eccentricity right after a long-eccentricity minimum, culminating during a short-eccentricity maximum at the F-F boundary.

An astronomical age model encompassing 5.67-Myr is constructed based on the recovered eccentricity imprint on TOC. The floating astrochronology provides new estimates for the duration of the Rhinestreet, LKW, and UKW events as well as the Kellwasser Crisis interval. These align with current estimates from coeval, globally distributed sections. Finally, the floating astrochronology is put into the Frasnian astrochronozonal framework of Whalen et al. (2017) and De Vleeschouwer et al. (2017), further putting the WVC record into a global and astronomical context. Future work may further refine the proposed astrochronology by increasing data resolution, thereby allowing resolving precession and short obliquity. In addition, this approach would enable an investigation into the extent to which eccentricity-modulated precession controls anoxia development, as well as whether short-obliquity forcing contributed to the stark transgressions associated with the Kellwasser events. Nevertheless, other potential mechanisms should also be considered to fully capture the complexity of these sea-level fluctuations during this key interval.

This cyclostratigraphic investigation of the Upper Devonian WVC highlights the intricate interplay of Milankovitch cycles and their effect on the Rhinestreet and Kellwasser events. By integrating existing models of anoxia, sea-level change and astronomical forcing, this study advances our understanding of the causal mechanisms that shaped these key intervals in Earth's history.

Acknowledgments

Carlton E. Brett, David De Vleeschouwer and Damien Pas are acknowledged for insightful discussions on the Devonian of New York State (USA), Devonian anoxic events and cyclostratigraphy.

Funding sources

This is a contribution to the "Projet de Recherche" funded by the Belgian National Fund of Sciencific Research (FNRS), contract T.0037.22 "WarmAnoxia". Michiel Arts is financially supported by the FNRS-PDR T.0051.19 grant "SiluCarb". FNRS had no involvement in the study design, analysis and interpretation of data, writing of the manuscript or decision to submit this study for publication.

Author contributions

Jarno J.C. Huygh: Conceptualization, Formal analysis, Investigation, Methodology, Visualization, Writing – original draft. Thomas J. Algeo: Conceptualization, Data curation, Methodology, Project administration, Resources, Supervision, Writing – review and editing. Bradley B. Sageman: Conceptualization, Data curation, Project administration, Resources, Supervision, Writing – review and editing. Michiel Arts: Conceptualization, Formal Analysis, Investigation, Methodology, Writing – review and editing. Charles A. Ver Straeten: Data curation, Formal analysis, Investigation, Writing – review and editing. D. Jeffrey Over: Formal analysis, Investigation, Visualization, Writing – review and editing. Justin Gérard: Conceptualization, Writing – review and editing. Loïc Sablon: Conceptualization, Writing – review and editing. Michel Crucifix: Conceptualization, Funding acquisition, Methodology, Project administration, Resources, Supervision, Writing – review and editing. Anne-Christine Da Silva: Conceptualization, Formal Analysis, Funding acquisition, Investigation, Methodology, Project administration, Resources, Supervision, Writing – review and editing.

References

Algeo, T. J. and Liu, J., 2020. A re-assessment of elemental proxies for paleoredox analysis. *Chem. Geol.*; 540, 119549. https://doi.org/10.1016/j.chemgeo.2020.119549.

Algeo, T. J., and Lyons, T. W., 2006. Mo–total organic carbon covariation in modern anoxic marine environments: Implications for analysis of paleoredox and paleohydrographic conditions, *Paleoceanogr.;* 21, PA1016, doi:10.1029/2004PA001112.

Algeo, T. J. and Scheckler, S. E., 1998. Terrestrial–marine teleconnections in the Devonian: links between the evolution of land plants, weathering processes, and marine anoxic events. *Phil. Trans*; 353, 113–130.

Algeo, T. J. and Scheckler, S. E., 2010. Land plant evolution and weathering rate changes in the Devonian. *J. Earth Sci.*; 21, 75-78. doi:10.1007/s12583-010-0173-2.

Algeo, T. J., and Shen, J., 2024. Theory and classification of mass extinction causation. *Natl. Sci. Rev.,* 11, nwad237. doi:10.1093/nsr/nwad237.

Algeo, T. J., Berner, R. A., Maynard, J. B., Scheckler, S. E., 1995. Late Devonian oceanic anoxic events and biotic crises: “rooted” in the evolution of vascular land plants? *GSA Today* 5, 3, 45-66.

Algeo, T. J., Maynard, J. B., Scheckler, S. E., 2001. Effects of the Middle to Late Devonian spread of vascular land plants on weathering regimes, marine biotas, and global climate. In: Gensel, P. G., Edwards, D. (Eds.), Plants Invade the Land, chapter 12, 213-236. doi:10.7312/gens11160-013

Algeo, T. J., Remírez, M. N., Zhao, H. Schwark, L., Gordon, G., Anbar, A., Bates, S., Lyons, T., Over, D.J., , Sageman, B. B., 2025. Transient glacio-eustatic fall and its climato-environmental effects during the Frasnian-Famennian transition. *Glob. Planet. Change – this issue*.

Alvarez, L. W., Alvarez, W., Asaro, F., Michel, H. V., 1980. Extraterrestrial Cause for the Cretaceous-Tertiary Extinction. *Science*; 208, 4448, 1095-1108. doi: 10.1126/science.208.4448.1095.

Arts, M.C.M., 2023. WaverideR: Extracting Signals from Wavelet Spectra. https://CRAN.R-project.org/package=WaverideR

Arts, M.C.M., Corradini, C., Pondrelli, M., Pas, D., Da Silva, A.-C., 2024. Age and orbital forcing in the upper Silurian Cellon section (Carnic Alps, Austria) uncovered using the WaverideR R package. *Front. Earth Sci.*, 12, https://doi.org/10.3389/feart.2024.1357751

Averbuch, O., Tribovillard, N., Devleeschouwer, X., Riquier, L., Mistiaen, B., Van Vliet-Lanoe, B., 2005. Mountain building-enhanced continental weathering and organic carbon burial as major causes for climatic cooling at the Frasnian–Famennian boundary (c. 376 Ma)? *Terra Nova*; 17; 1, 25-34. doi:10.1111/j.1365-3121.2004.00580.x

Becker, R. T., Marshall, J. E. A., Da Silva, A.-C., 2020. The Devonian Period. In: Gradstein, F. M., Ogg, J. G., Schmitz, M. D. And Ogg, G. (Eds.), *The Geologic Time Scale 2020*, chapter 22, 733-810. https://doi.org/10.1016/B978-0-12-824360-2.00022-X.

Bennet, W. W., Canfield, D. E., 2020. Redox-sensitive trace metals as paleoredox proxies: A review and analysis of data from modern sediments. *Earth Sci. Rev.*; 204, 103175. https://doi.org/10.1016/j.earscirev.2020.103175.

Berger, A. L., 1973. La théorie astronomique des paléoclimats, PhD thesis, p315, Université catholique de Louvain. https://hdl.handle.net/2078.1/233872

Berger, A. L., 1987. Long-term variations of caloric insolation resulting from the Earth's orbital elements. *Quat. Res.*; 9, 139-167.

Berger, A. L., 1988. Milankovitch Theory and Climate. *Rev. Geophys.*; 26, 4, 624-657. https://doi.org/10.1029/RG026i004p00624

Bretagnon, P., 1974. Termes à longues périodes dans le système solair, *Astron. Astroph.*, 30, 141-154.

Brett, C. E., Zambito, J. J. IV, McLaughlin, P. I., Emsbo, P., 2020. Revised perspectives on Devonian biozonation and environmental volatility in the wake of recent time-scale revisions. *Palaeogeogr. Palaeoclimatol. Palaeoecol.*; 549, 108843. https://doi.org/10.1016/j.palaeo.2018.06.037.

Calvert, S. E. and Pedersen, T. F., 2007. Elemental proxies for palaeoclimatic and palaeoceanographic variability in marine sediments: interpretation and application. In: Hillaire-Marcel, C. and De Vernal, A. (Eds.), Proxies in late Cenozoic Paleoceanography, chapter 14, *Dev. In Mar. Geol.*; 1, 567-643. ISSN 1572-5480, doi:10.1016/S1572-5480(07)01019-6.

Carmichael, S. K., Waters, J. A., Königshof, P., Suttner, T. J., Kido, E., 2019. Paleogeography and paleoenvironments of the Late Devonian Kellwasser event: A review of its sedimentological and geochemical expression. *Glob. Planet. Change*; 183, 102984. https://doi.org/10.1016/j.gloplacha.2019.102984.

Croudace, I. W. and Rothwell, R. G., 2015. Micro-XRF studies of sediment cores, Applications of a non-destructive tool for the environmental sciences. In: Smol, J. P. (Ed.), *Dev. in Paleoenv. Res.*; 17, ISSN 1571-5299.

Da Silva, A.-C., Sinnesael, M., Claeys, P., Davies, J. H. F. L., de Winter, N. J., Percival, L. M. E., Schaltegger, U., De Vleeschouwer, D., 2020. Anchoring the Late Devonian mass extinction in absolute time by integrating climatic controls and radio-isotopic dating. *Sci. Rep.*; 10, 12940. https://doi.org/10.1038/s41598-020-69097-6.

De Vleeschouwer, D., Da Silva, A.-C., Boulvain, F., Crucifix, M. & Claeys, P., 2012. Precessional and half-precessional climate forcing of Mid-Devonian monsoon-like dynamics. *Clim. Past.*; 8, 337–351.

De Vleeschouwer, D., Rakociński, M., Racki, G., Bond, D. P. G., Sobień, K., Claeys, P., 2013. The astronomical rhythm of Late-Devonian climate change (Kowala section, Holy Cross Mountains, Poland). *Earth Planet. Sci. Lett.*; 365, 25-37. http://dx.doi.org/10.1016/j.epsl.2013.01.016.

De Vleeschouwer, D., Crucifix, M., Bounceur, N. & Claeys, P., 2014. The impact of astronomical forcing in the Late Devonian greenhouse climate. *Glob. Planet. Change*; 120, 65–80.

De Vleeschouwer, D., Da Silva, A.-C., Sinnesael, M., Chen, D., Day, J. E., Whalen, M. T., Guo, Z., Claeys, P., 2017. Timing and pacing of the Late Devonian mass extinction event regulated by eccentricity and obliquity. *Nat. Comm.*; 8, 2268. doi:10.1038/s41467-017-02407-1.

De Vleeschouwer, D., Percival, L. M. E., Wichern, N. M. A., Batenburg, S. J., 2024. Pre-Cenozoic cyclostratigraphy and palaeoclimate responses to astronomical forcing. *Nat. Rev. Earth Environ.*; 5, 56-75. https://doi.org/10.1038/s43017-023-00505-x.

d-maps.com, State of New York map. Last accessed via: https://d-maps.com/pays.php?num_pay=379&num_pag=1&lang=en on April 7th, 2025.

Gérard, J., Sablon, L., Huygh, J. J. C., Da Silva, A.-C., Pohl, A., Vérard, C., Crucifix, M., 2025. Exploring the mechanisms of Devonian oceanic anoxia: impact of ocean dynamics, palaeogeography, and orbital forcing. *Clim. Past*; 21, 239-260. https://doi.org/10.5194/cp-21-239-2025.

Gérard, J., Pohl, A., Sablon, L., Huygh, J. J. C., Da Silva, A.-C., Crucifix, M., (in review). Spatially contrasted response of Devonian anoxia to astronomical forcing. *EGUsphere*, 2025-4238 (preprint). https://doi.org/10.5194/egusphere-2025-4238

Hays, J. D., Imbrie, J. & Shackleton, N. J., 1976. Variations in the Earth's orbit: pacemaker of the ice ages. *Science* 194, 1121–1132.

Hilgen, F., Lourens, L., and Pälike, H., 2020. Should unit-stratotypes and astrochronozones be formally defined? A dual proposal (including postscriptum). *Newsl. Stratigr.*; 53, 19.

Hinnov, L. A., 2000. New perspectives on orbitally forced stratigraphy. *Annu. Rev. Earth Planet. Sci.,* 28, 419-475. doi:10.1146/annurev.earth.28.1.419

Hinnov, L. A., 2013. Cyclostratigraphy and its revolutionizing applications in the Earth and planetary sciences. *Geol. Soc. Am. Bull.*; 125, 1703–1734.

Huang, C., Joachimski, M. M., Gong, Y., 2018. Did climate changes trigger the Late Devonian Kellwasser Crisis? Evidence from high-resolution conodont $\delta^{18}O_{PO4}$ record from South China. *Earth Planet. Sci. Lett.*; 495, 174-184. https://doi.org/10.1016/j.epsl.2018.05.016.

Jaminski, J., Algeo, T.J., Maynard, J.B., Hower, J.C., 1998. Climatic origin of dm-scale compositional cyclicity in the Cleveland Member of the Ohio Shale (Upper Devonian), Central Appalachian Basin, USA. In: Schieber, J., et al. (eds.), *Shales and Mudstones*, *vol. 1*, Schweizerbart'sche, Stuttgart, Germany, 217-242.

Joachimski, M.M. and Buggisch, W., 2002. Conodont apatite $\delta^{18}O$ signatures indicate climatic cooling as a trigger of the Late Devonian mass extinction. *Geology*; 30: 711-714. https://doi.org/10.1130/0091-7613(2002)030<0711:CAOSIC>2.0.CO;2.

Kabanov, P., Hauck, T. E., Gouwy, S. A., Grasby, S. E., van der Boon, A., 2023. Oceanic anoxic events, photic-zone euxinia, and controversy of sea-level fluctuations during the Middle-Late Devonian. *Earth Sci. Rev.*; 241, 104415. https://doi.org/10.1016/j.earscirev.2023.104415.

Lash, G. G. and Blood, D. R., 2006. The Upper Devonian Rhinestreet black shale of western New York State – evolution of a hydrocarbon system. In: 78th Meeting, New York State Geological Association, Sunday B1 field trip, p. 223-289.

Laskar, J., 1990. The chaotic motion of the solar system: A numerical estimate of the size of the chaotic zones, *Icarus*, 88, 266-291. doi:10.1016/0019-1035(90)90084-m

Laskar, J., 2020. Astrochronology. In: Gradstein, F. M., Ogg, J. G., Schmitz, M. D. And Ogg, G. (Eds.), *The Geologic Time Scale 2020*, chapter 4, 139-158.

Laskar, J., Robutel, P., Joutel, F., Gastineau, M., Correia, A. C. M., Levrard, B., 2004. A long-term numerical solution for the insolation quantities of the Earth. *Astron. Astrophys.*; 428, 1, 261-285. https://doi.org/10.1051/0004-6361:20041335.

Li, M., Hinnov, L. A., Huang, C., Ogg, J. G., 2018. Sedimentary noise and sea levels linked to land–ocean water exchange and obliquity forcing. *Nat. Comm.*; 9, 1004. doi:10.1038/s41467-018-03454-y.

Liu, J.S., Algeo, T.J., Jaminski, J., Kuhn, T., Joachimski, M.M., 2019. Evaluation of high-frequency paleoenvironmental variation using an optimized cyclostratigraphic framework: Example for CS-Fe analysis of Devonian-Mississippian black shales (Central Appalachian Basin, USA). *Chem. Geol.*, *525*, 303-320.

Lourens, L. J., Hilgen, F. J., 1997. Long-periodic variations in the Earth's obliquity and their relation to third-order eustatic cycles and late Neogene glaciations. *Quat. Int.*; 40, 43-52.

Lu, M., Lu, Y., Ikejiri, T., Sun, D., Carroll, R., Blair, E.H., Algeo, T.J. and Sun, Y., 2021. Periodic oceanic euxinia and terrestrial fluxes linked to astronomical forcing during the Late Devonian Frasnian–Famennian mass extinction. *Earth and Planetary Science Letters*, 562, 116839.

Ma, K., Hinnov, L. A., Zhang, X., Gong, Y., 2022. Astronomical climate changes trigger Late Devonian bio- and environmental events in South China. *Glob. Planet. Change*; 215, 103874. https://doi.org/10.1016/j.gloplacha.2022.103874.

McLennan, S. M., 2001. Relationships between the trace element composition of sedimentary rocks and upper continental crust. *Geochem. Geophys. Geosyst.*; 2, 2000GC000109. https://doi.org/10.1029/2000GC000109.

Meyers, S.R., 2014. Astrochron: An R Package for Astrochronology. https://cran.r-project.org/package=astrochron

Meyers, S. R., 2015. The evaluation of eccentricity-related amplitude modulation and bundling in paleoclimate data: An inverse approach for astrochronologic testing and time scale optimization. *Paleoceanogr.*; 30, 12, 1625-1640. https://doi.org/10.1002/2015PA002850.

Meyers, S. R., 2019. Cyclostratigraphy and the problem of astrochronologic testing. *Earth Sci. Rev.*; 190, 190-223. https://doi.org/10.1016/j.earscirev.2018.11.015.

Meyers, S. R. and Hinnov, L. A., 2010. Northern Hemisphere glaciation and the evolution of Plio-Pleistocene climate noise. *Paleoceanogr.*; 25, PA3207. doi:10.1029/2009PA001834.

Miller, K. G., Kominz, M. A., Browning, J. V., Wright, J. D., Mountain, G. S., Katz, M. E., Sugarman, P. J., Cramer, B. S., Cristie-Blick, N., Pekar, S. F., 2005. The Phanerozoic Record of Global Sea-Level Change. *Science*; 310, 1293-1298. doi: 10.1126/science.1116412.

Mudelsee, M., 2010. Climate Time Series Analysis, Classical statistical and bootstrap methods. ISSN 1383-9601.

Murphy, A. E., Sageman, B. B., Hollander, D. J., 2000. Eutrophication by decoupling of the marine biogeochemical cycles of C, N, and P: A mechanism for the Late Devonian mass extinction. *Geology*; 28, 5, 427-430.

Over, D. J., 1997. Conodont biostratigraphy of the Java Formation (Upper Devonian) and the Frasnian-Famennian boundary in western New York State. *GSA Spec. Pap.*; 321.

Over, D. J., Baird, G. C., Kirchgasser, W. T., 2023. The Frasnian Strata - Lower Upper Devonian – of New York State. Chapter 1 in: Ver Straeten, C.A., Over D. J., and Woodrow, D. (Eds.), Devonian of New York, Volume

3: Frasnian to Famennian (Upper Devonian) stages and the Devonian terrestrial system in New York, , *Bull. Am. Paleontol.;* 1-28. doi:10.32857/bap.2023.407.01.

Percival, L.M.E., Davies, J. H. F. L., Schaltegger, U., De Vleeschouwer, D., Da Silva, A.-C., Föllmi, K. B., 2018. Precisely dating the Frasnian-Famennian boundary: implications for the cause of the Late Devonian mass extinction. *Sci. Rep.*; 8, 9578. doi:10.1038/s41598-018-27847-7.

Percival, L. M. E., Selby, D., Bond, D. P. G., Rakociński, M., Racki, G., Marynowski, L., Adatte, T., Spangenberg, J. E., Föllmi, K. B., 2019. Pulses of enhanced continental weathering associated with multiple Late Devonian climate perturbations: Evidence from osmium-isotope compositions. *Palaeogeogr. Palaeoclimatol. Palaeoecol.*; 524, 240-249.

Percival, L. M. E., Selby, D., Bond, D. P. G., Rakociński, M., Marynowski, L., Hood, A. v. S., Addate, T., Spangenberg, J. E., Föllmi, K. B., 2020. Phosphorus-cycle disturbances during the Late Devonian anoxic events. *Glob. Planet. Change*; 184, 103070. https://doi.org/10.1016/j.gloplacha.2019.103070.

Pisarzowska, A. and Racki, G., 2020. Comparative carbon isotope chemostratigraphy of major Late Devonian biotic crises, chapter 8. *Stratigr. Timescales*; 5, 387-466.

Racki, G. A., 2020. Volcanic scenario for the Frasnian–Famennian major biotic crisis and other Late Devonian global changes: more answers than questions? *Glob. Planet. Change;* 189, 103174. https://doi.org/10.1016/j.gloplacha.2020.103174.

Raup, D. M. and Sepkoski, J. J., Jr., 1982. Mass extinctions in the marine fossil record. *Science;* 215, 4539, 1501-1503. doi:10.1126/science.215.4539.1501.

Reershemius, T. and Planavsky, N. J., 2021. What controls the duration and intensity of ocean anoxic events in the Paleozoic and Mesozoic? *Earth Sci. Rev.*; 221; 103787. https://doi.org/10.1016/j.earscirev.2021.103787.

Sageman, B. B., Murphy, A. E., Werne, J. P., Ver Straeten, C. A., Hollander, D. J., Lyons, T. W., 2003. A tale of shales: the relative roles of production, decomposition, and dilution in the accumulation of organic-rich strata, Middle–Upper Devonian, Appalachian basin. *Chem. Geol.*; 195, 229-273. doi:10.1016/S0009-2541(02)00397-2.

Schindler, E., 1990. The late Frasnian (Upper Devonian) Kellwasser Crisis. In: Kauffman, E.G., Walliser, O.H. (Eds.), Extinction Events in Earth History: Proceedings of the Project 216: *Global Biological Events in Earth History*; 151–159. https://doi.org/10.1007/BFb0011143.

Schindler, E., 1993. Event-stratigraphic markers within the Kellwasser Crisis near the Frasnian/Famennian boundary (Upper Devonian) in Germany. *Palaeogeogr. Palaeoclimatol. Palaeoecol.*; 104, 1, 115–125.

Smart, M. S., Filippelli, G., Gilhooly, W. P. III, 2023. Enhanced terrestrial nutrient release during the Devonian emergence and expansion of forests: evidence from lacustrine phosphorus and geochemical records. *Geol. Soc. Am. Bull.*; 135: 1879-1898. https://doi.org/10.1130/B36384.1.

Smith, D. G., 2023. The Orbital Cycle Factory: Sixty cyclostratigraphic spectra in need of re-evaluation. *Palaeogeogr. Palaeoclimatol. Palaeoecol.*; 628, 111744. https://doi.org/10.1016/j.palaeo.2023.111744.

Smith, G. J. and Jacobi, R. D., 2023. Upper Frasnian and Famennian stratigraphy in western New York State. Chapter 3 in: Ver Straeten, C.A., Over D. J., and Woodrow, D. (Eds.), Devonian of New York, Volume 3: Frasnian to Famennian (Upper Devonian) stages and the Devonian terrestrial system in New York, *Bull. Am. Paleontol.;* 47-111. doi:10.32857/bap.2023.407.03.

Tribovillard, N., 2021. Re-assessing copper and nickel enrichments as paleoproductivity proxies. *Earth Sci. Bull.*; 192, 54. https://doi.org/10.1051/bsgf/2021047.

Tribovillard, N., Algeo, T. J., Lyons, T. W., Riboulleau, A., 2006. Trace metals as paleoredox and paleoproductivity proxies: An update. *Chem. Geol.*; 232, 12-32. doi:10.1016/j.chemgeo.2006.02.012.

Van Cappellen, P. and Ingall, E. D., 1994. Benthic phosphorus regeneration, net primary production, and ocean anoxia: A model of the coupled marine biogeochemical cycles of carbon and phosphorus. *Paleoceanography*, 9, 5, 677-692. https://doi.org/10.1029/94PA01455

Van der Weijden, C. H., 2002. Pitfalls of normalization of marine geochemical data using a common divisor. *Mar. Geol.*; 184, 167-187.

Ver Straeten, C. A., 2009. The classic Devonian of the Catskill Front: A foreland basin record of Acadian Orogenesis. In: Vollmer, F. (Ed), New York State Geological Association, 81st Annual Meeting Guidebook; 7, 1-54.

Ver Straeten, C. A., 2010. Lessons from the foreland basin: Appalachian basin perspectives on the Acadian orogeny. In: Tollo, R.P., Bartholomew, M.J., Hibbard, J.P. and Paul M. Karabinos, P.M. (Eds.), From Rodinia to Pangea: The Lithotectonic Record of the Appalachian Region, *Geol. Soc. Am.*, 206, 251-282.

Ver Straeten, C. A., 2023. An introduction to the Devonian Period, and the Devonian in New York State and North America. In: Ver Straeten, C. A., Over, D. J. and Woodrow, D. (Eds.), Devonian of New York, Volume 1: Introduction and Přídolí to lower Givetian (Upper Silurian to Middle Devonian) stages. *Bull. Am. Paleontol.;* 403-404. doi:10.32857/bap.2023.403.03.

Ver Straeten, C. A., Brett, C. E., Sageman, B. B., 2011. Mudrock sequence stratigraphy: A multi-proxy (sedimentological, paleobiological and geochemical) approach, Devonian Appalachian Basin. *Palaeogeogr. Palaeoclimatol. Palaeoecol*.; 304, 54-73. doi:10.1016/j.palaeo.2010.10.010.

Ver Straeten, C. A., Over, D. J., Baird, G. C., 2020. Arc-to-craton: Devonian air-fall tephras in the eastern United States. In: Avary, K. L., Hasson, K. O. and Diecchio, R. J. (Eds.), The Appalachian Geology of John M. Dennison: Rocks, People, and a Few Good Restaurants along the Way. *Geol. Soc. Am. Spec. Pap.*; 545, 35-53. https://doi.org/10.1130/2020.2545(03).

Walliser, O. H., 1996. Global events and event stratigraphy. ISBN-13: 978-3-642-79636-4. Springer*;* 225-250. doi:10.1007/978-3-642-79634-0.

Wang, X., Liu, S.-A., Wang, Z., Chen, D., Zhang, L., 2018. Zinc and strontium isotope evidence for climate cooling and constraints on the Frasnian-Famennian (~372 Ma) mass extinction. *Palaeogeogr. Palaeoclimatol. Palaeoecol*.; 498, 68-82. https://doi.org/10.1016/j.palaeo.2018.03.002.

Weedon, G. P., 2022. Problems with the current practice of spectral analysis in cyclostratigraphy: Avoiding false detection of regular cyclicity. *Earth Sci. Rev.*; 235, 104261. https://doi.org/10.1016/j.earscirev.2022.104261.

Whalen, M. T., De Vleeschouwer, D., Payne, J. H., Day, J. E., Over, D. J., Claeys, P., 2017. Pattern and timing of the Late Devonian biotic crisis in western Canada: Insights from carbon isotopes and astronomical calibration of magnetic susceptibility data. In: Playton, T. E., Kerans, C., Weissenberger, J. A. W. (Eds.), New advances in Devonian carbonates: Outcrop analogs, reservoirs and chronostratigraphy, *SEPM*; 107, 185-201. ISBN 978-1-56576-344-9. https://doi.org/10.2110/sepmsp.107

Wichern, N. M. A., Bialik, O. M., Nohl, T., Percival, L. M. E., Becker, T. R., Kaskes, P., Claeys, P., De Vleeschouwer, D., 2024. Astronomically paced climate and carbon cycle feedbacks in the lead-up to the Late Devonian Kellwasser Crisis. *Clim. Past;* 20, 415-448. https://doi.org/10.5194/cp-20-415-2024

Wigley, T. M. L., 1976, Spectral analysis and the astronomical theory of climatic change, *Nature*, 264, 629–631, doi:10.1038/264629a0

Zeebe, R. E. and Lantink, M. L., 2024. A secular solar system resonance that disrupts the dominant cycle in Earth's orbital eccentricity (g_2-g_5): Implications for astrochronology. *Astron. J.*; 167:204. https://doi.org/10.3847/1538-3881/ad32cf.

Zeebe, R. E. and Kocken, I. J., 2025. Applying astronomical solutions and Milanković forcing in the Earth sciences. *Earth Sci. Rev.*; 261, 104959. https://doi.org/10.1016/j.earscirev.2024.104959

Zeeden, C., Meyers, S., Hilgen, F., Lourens, L., Laskar, J., 2019. Time scale evaluation and the quantification of obliquity forcing. *Quat. Sci. Rev.*; 209, 100-113. https://doi.org/10.1016/j.quascirev.2019.01.018.

Supplemental information

A. R-script and research data

All will be made available to the Reviewers and will be accessible online after acceptance of this manuscript.

B. Proxies

Total Organic Carbon—Total organic carbon (TOC), a proxy for the flux, accumulation and preservation of OM (Sageman et al., 2003; Ver Straeten et al., 2011), varies from 0.00 to 4.75 % throughout the record. The highest values are recorded in the black shales of the basal Rhinestreet Formation as well as the Pipe Creek Formation (LKW) and Hanover Formation (incl. UKW) (Fig. 2). Petrographic studies indicate that the majority of OM in Appalachian Basin Devonian black shales originated from the marine realm (Jaminski et al., 1998; Sageman et al., 2003). As a prime indicator for marine anoxic events in semi-restricted basins (Carmichael et al., 2019), the TOC proxy signal is the primary target for cyclostratigraphy, with the goal of determining whether these events and their pacing are astronomically forced (cf. Liu et al., 2025).

Detrital Input (Ti)—Titanium is a conservative, redox-insensitive, diagenetically resistant element that is associated with the coarse-grained, detrital fraction of the sedimentary record and is commonly transported from the continent into the ocean (Calvert and Pedersen, 2007; Croudace and Rothwell, 2015). For the Appalachian foreland Basin, the majority of Ti originated from dense, silt-to-sand-sized grains from the surrounding Euramerican continent and is interpreted to reflect increased influx of coarse-grained material due to reduced monsoonal activity during periods of increased aridity (;Jaminski et al., 1998; Liu et al., 2019; Wichern et al., 2024). Most likely, the prograding Catskill Delta complex as a result of the Acadian Orogeny further contributed to the Ti-budget (Ver Straeten, 2009; Smith and Jacobi, 2023).

Sea Level (Ti/Al)—Often, elemental proxy concentrations are normalized versus immobile elements such as Al to account for facies changes, dilution, etc. (Calvert and Pedersen, 2007; Croudace and Rothwell, 2015), which has proven useful for interpreting geochemical element profiles (Van der Weijden, 2002). Moreover, normalization to Al is also utilized for the calculation of trace-metal enrichment factors (Algeo and Liu, 2020; McLennan, 2001; Tribovillard, 2021). Here, both Ti and Al can be attributed to the detrital fraction of the sediment.

Generally, Ti/Al is interpreted as a sedimentary grain-size proxy (Calvert and Pedersen, 2007). Grain-size variations may be the result of a wide range of paleoclimatic and paleoenvironmental changes, such as a shift in climatic conditions (e.g. wet/dry cycles) causing a shift in eolian versus fluvial influx (Croudace and Rothwell, 2015; Lourens et al., 2001) or eustatic sea-level variations (Calvert and Pedersen, 2007; Chen et al., 2013). Specifically for the West Valley core, the Ti/Al ratio is interpreted – based on geochemical and petrographic data – to reflect relative sea-level changes and related aggradation/progradation (Sageman et al., 2003). Thus, an increase Ti/Al is interpreted to primarily reflect progradation and relative sea-level fall (and vice-versa). In addition, trends in Ti/Al match well with regional stratigraphic trends (Sageman et al., 2003), further justifying its use as a proxy for sea-level change. Yet, a minor eolian contribution to variations in the Ti/Al signal is not excluded by Sageman et al. (2003). Therefore, it is highly likely that Ti/Al represents an amalgamated signal, containing long-term global signals (e.g. sea level changes) with superimposed shorter-term regional-to-global changes in the composition of terrigenous influx (e.g. due to increased aeolian supply).

Trace Metal Proxies—A plethora of trace metal paleoredox proxies are readily available from the geochemical dataset by Sageman et al. (2003). In this study, three proxies are included that provide insight on paleoredox conditions, as well as paleoproduction and -hydrography.

Ni_{EF} is an efficacious proxy across the redox-spectrum and can be strongly enriched under sulfate-reducing conditions (Algeo and Liu, 2020). This enrichment factor was calculated as:

Ni_{EF} = [$(Ni/Al)_{sample}/(Ni/Al)_{upper\ crust}$] according to McLennan (2001) using Al_{crust} = 8.04% and Ni_{crust} = 44 ppm. In addition, re-assessment of the geochemical database of Algeo and Liu (2020) by Tribovillard (2021) highlights that Ni_{EF} equally has merit as a paleoproductivity proxy. Enrichment of Ni in association with other paleoredox proxies (e.g., V, Mo) and elevated TOC-values indicate paleoproductivity and anoxia were intertwined (Tribovillard et al., 2006). Conversely, absence of Ni in otherwise anoxic sediment may be explained by restricted water-mass renewal or stagnation (Tribovillard et al., 2006). Thus, an increase in Ni_{EF} is interpreted to reflect increased paleoproductivity and, if accompanied by an increase of other paleoredox proxies, a decrease in bottom water oxygenation. The Pearson's correlation indicates positive correlation between Ni_{EF} and TOC (r = +0.67, $p < 2.2e^{-16}$).

Sedimentary Mo is generally enriched in organic-rich marine facies deposited under anoxic conditions and is classically used as a benthic redox potential proxy, especially in association with other paleoredox proxies such as V (i.e., paleoredox proxy; Algeo and Lyons, 2006; Tribovillard et al., 2006) Typically, Mo burial peaks in weakly sulfidic paleoenvironments and is lower under strongly sulfidic conditions (see Algeo and Lyons, 2006). Hence, lower Mo-values during an anoxic interval may be indicative of stronger reducing (sulfidic) conditions. However, this proxy is highly susceptible to reservoir effects in anoxic silled basins (Algeo and Lyons, 2006), as was most likely – at least intermittently – the case for the Late Devonian Appalachian Basin (Algeo et al., 2025). As such, Mo/Al is also linked to hydrographic restriction of the deep-water mass and is therefore interpreted as an amalgamated signal. This interpretation is complemented by Mo/TOC (Algeo and Lyons, 2006). The Pearson's product-moment correlation indicates correlation between Mo/Al and TOC (r = 0.7342, $p < 2.2e^{-16}$).

V is considered a redox proxy with minimal detrital influence (Tribovillard et al., 2006), undergoing a two-step reduction process that is strongly dependent on the intensity of reducing conditions (Tribovillard et al., 2006). Through comparison of its covariation with other paleoredox proxies (e.g., Ni, Mo) and TOC, it enables distinguishing anoxic and euxinic paleoconditions (Tribovillard et al., 2006). The Pearson's product-moment correlation indicates moderate correlation between V/Al and TOC (r = 0.3838, p < 1.25e^{-09}).

Stable Carbon Isotopes—Carbon cycle perturbations are tracked using $\delta^{13}C_{org}$ (from Murphy et al., 2000; Sageman et al., 2003). A positive carbon isotope excursion (pCIE) is interpreted to reflect reservoir shifts (e.g., net atmospheric CO_2 drawdown and carbon burial) and can be associated with climatic cooling (and vice-versa) (Murphy et al., 2000; Algeo and Shen, 2024). Two pCIE's, reaching peak values of -26.88‰ and -26.92‰ ($\delta^{13}C_{org}$ ‰ vs. PDB) characterize the LKW and UKW, respectively (Sageman et al., 2003).

Phosphorus—The key role of phosphorus (P) during the Kellwasser Crisis as a limiting nutrient for primary production and, consequently, as a proxy for nutrient flux, has been thoroughly highlighted by Percival et al. (2020) for the WVC. Land-plant-mediated nutrient influx, combined with ocean circulation changes and upwelling as well as P-recycling in reducing sediment offer multiple mechanisms via which the global phosphorus cycle may have contributed to marine anoxia development and sustenance (Algeo and Scheckler, 1998; Murphy et al., 2000; Percival et al., 2020; Sageman et al., 2003).

C. eTimeOpt Analyses (TOC, Ti)

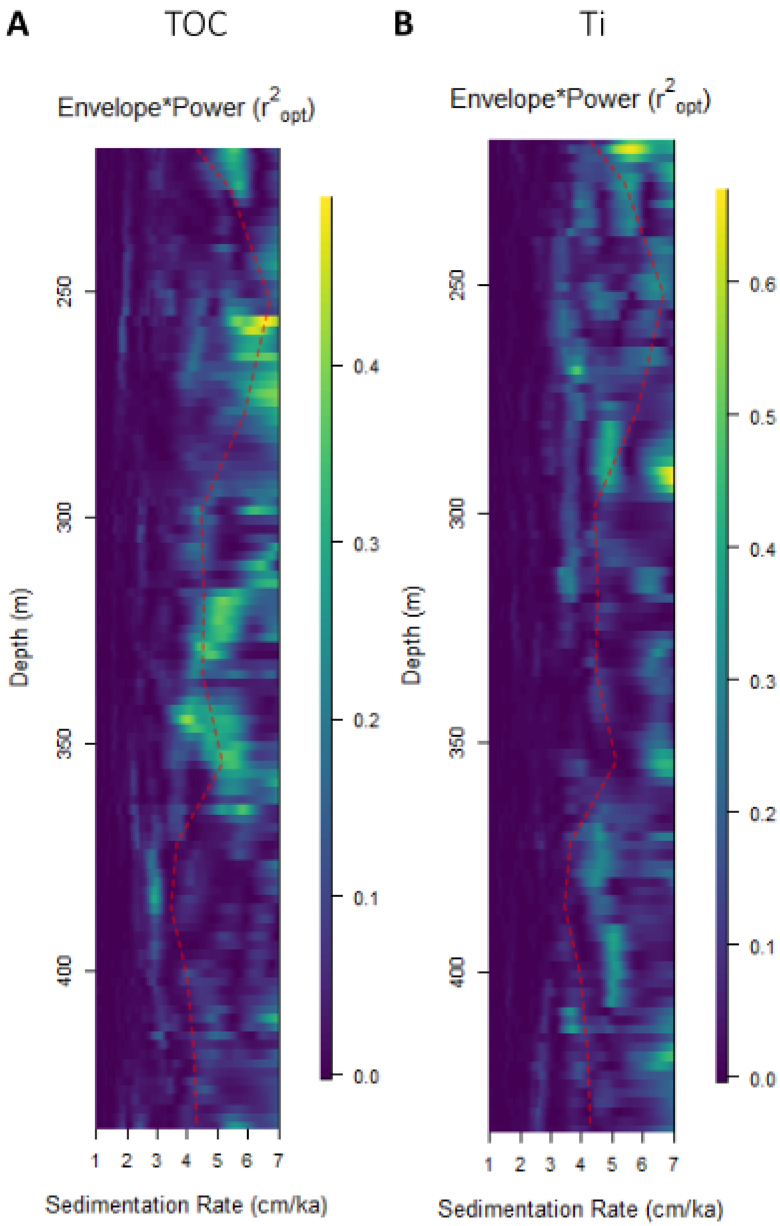

Fig. S1. eTimeOpt analysis of TOC and Ti. The ASR curve of the astronomical TOC age model is superimposed (dashed red).

D. Alternative Age Model (TOC)

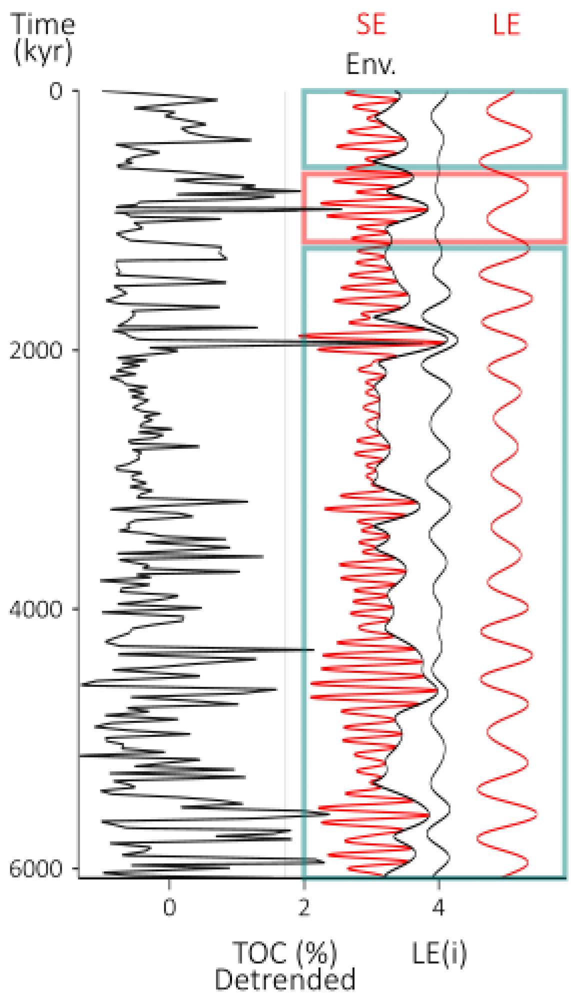

Fig. S2. Tuned TOC and eccentricity bandpass filter output. Detrended TOC (%, black), bandpass filters corresponding to 100-kyr SE (red), its envelope (black), 405-kyr LE(i) extracted from the envelope of SE (black), 405-kyr LE (red). Green boxes indicate a consistent phase relationship; the red box indicates an inconsistent phase relationship between the envelope of SE (LE(i)) and LE. Note relative time based on floating astrochronology.

E. *Time-Domain Cyclostratigraphy (Ti)*

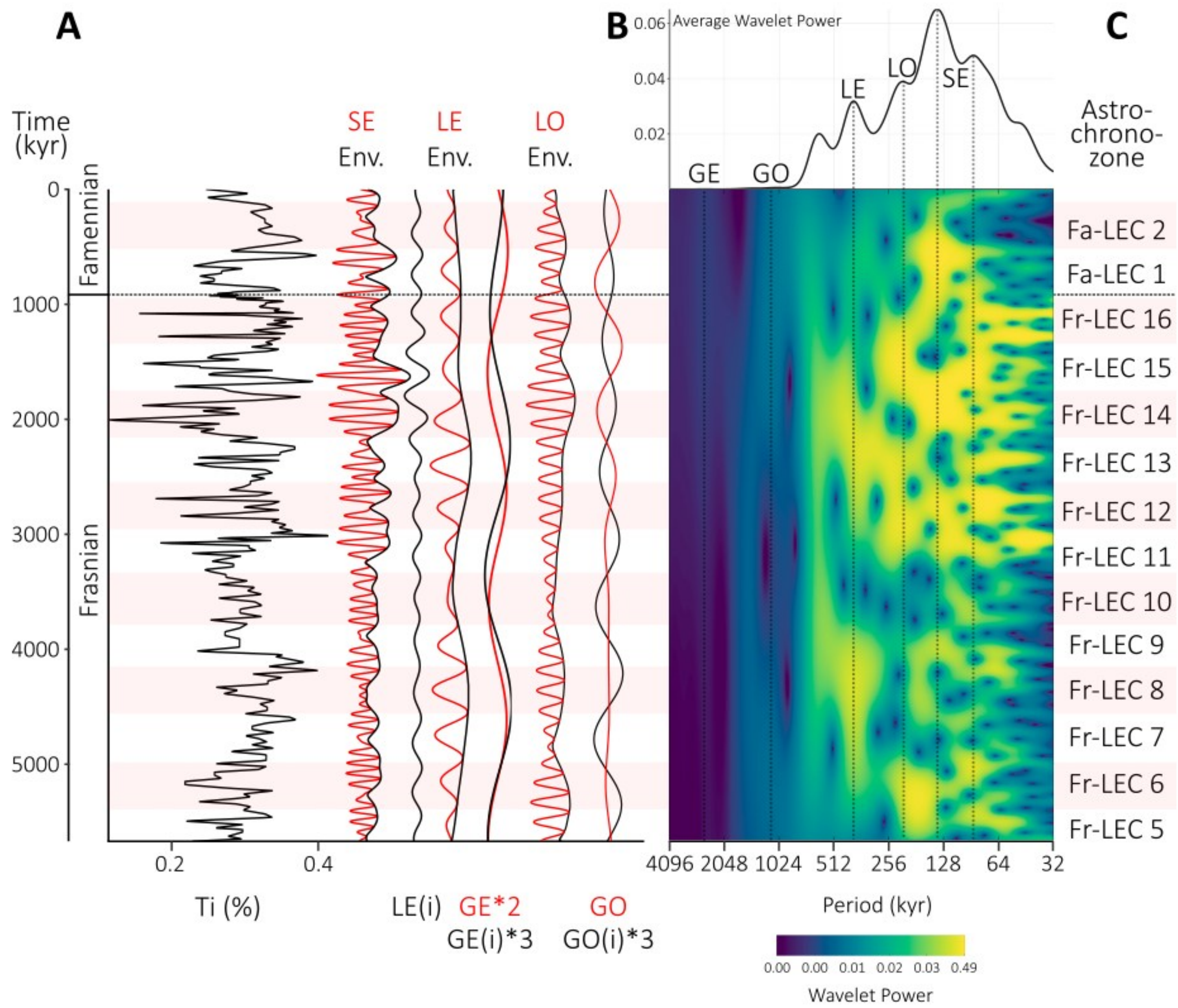

Fig. S3. Time-domain cyclostratigraphic analysis of Ti. A) Detrended Ti and bandpass filters corresponding to 100-kyr SE (red; 1/150 to 1/80 kyr^{-1}), its envelope (black), 405-kyr LE extracted from the envelope of SE (black; 1/505 to 1/305 kyr^{-1}), 405-kyr LE (red; 1/505 to 1/305 kyr^{-1}), its envelope (black), 2.4-Myr GE extracted from the envelope of GE (GE(i), black, scaled by factor 3; 1/2900 to 1/1900 kyr^{-1}), 2.4-Myr GE (red, scaled by factor 2; 1/2900 to 1/1900 kyr^{-1}), 173-kyr LO (red; 1/213 to 1/133 kyr^{-1}), its envelope (black), 1.2-Myr GO extracted from the envelope of LO (GO(i), black, scaled by factor 3; 1/1500 to 1/900 kyr^{-1}) and 1.2-Myr GO (red; 1/1500 to 1/900 kyr^{-1}), respectively. B) Average and evolutive wavelet periodogram. Target periodicities (kyr) indicated by dashed vertical lines for GE (2.4 Myr), GO (1.2 Myr), LE (405 kyr), LO (173 kyr) and SE (131 and 95 kyr, respectively). Note that both average and evolutive power spectra were calculated on detrended Ti to highlight higher frequency components (see R-script in Suppl. A for details). C) Assigned astrochronozones (Whalen et al., 2017; De Vleeschouwer et al., 2017). The cone of influence was removed from the wavelet periodogram for visual clarity (see Suppl. A). Note relative time based on floating astrochronology.

F. WVC Age-Depth Model

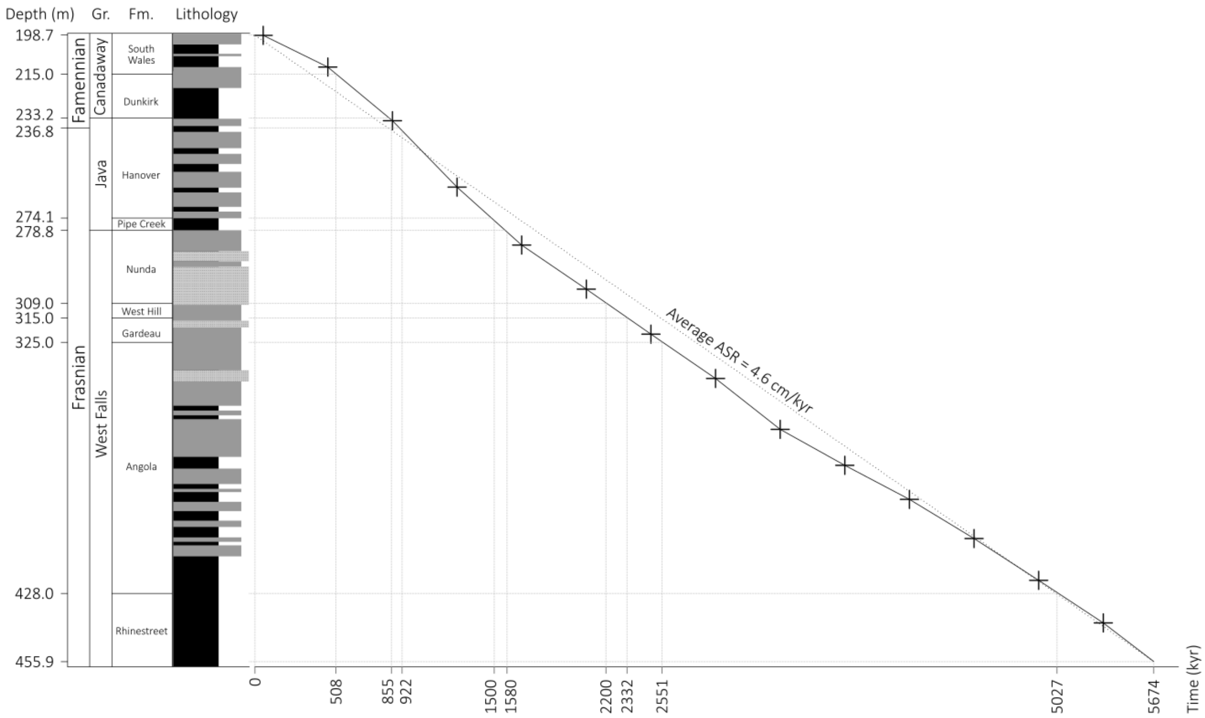

Fig. S4. Stratigraphy, lithostratigraphy and sedimentation rate curve. Note relative time based on floating astrochronology.

G. MTM spectra of redox-sensitive proxies

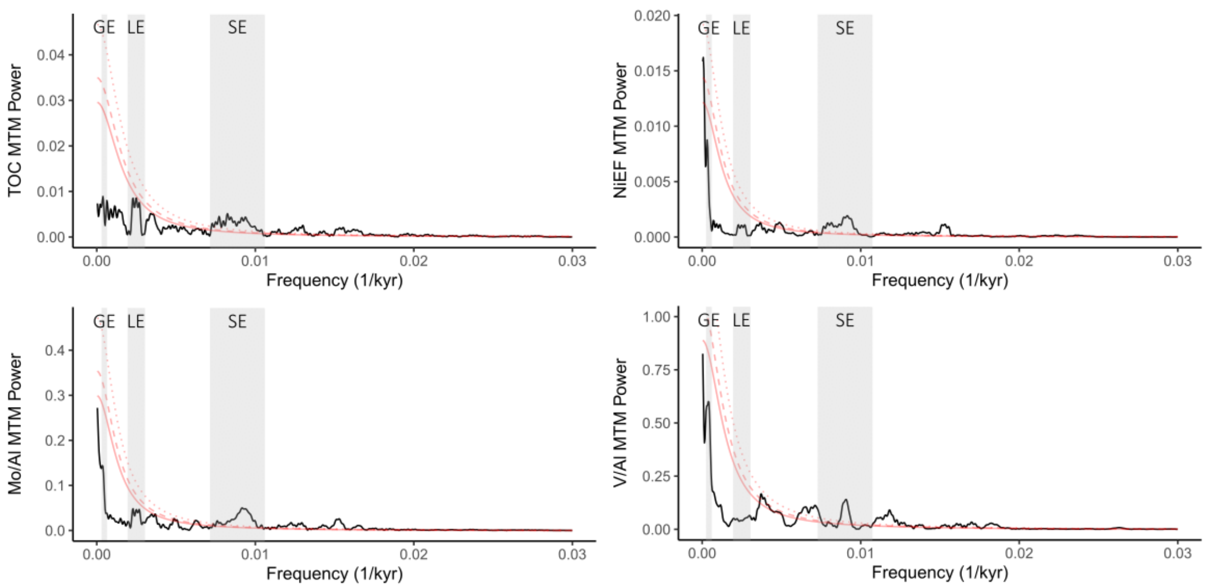

Fig. S5. Multitaper method (MTM) power spectra of TOC, NiEF, Mo/Al and V/Al. ~100-kyr short eccentricity (SE), 405-kyr long eccentricity (LE) and ~2.4-Myr Grand eccentricity (GE) marked by gray vertical lines. Full, dashed and dotted lines indicate AR1 90%, 95% and 99% confidence intervals, for indicative purposes only.

Supplemental References

Algeo, T. J. and Liu, J., 2020. A re-assessment of elemental proxies for paleoredox analysis. *Chem. Geol.*; 540, 119549. https://doi.org/10.1016/j.chemgeo.2020.119549.

Algeo, T. J., and Lyons, T. W., 2006. Mo–total organic carbon covariation in modern anoxic marine environments: Implications for analysis of paleoredox and paleohydrographic conditions, *Paleoceanogr.;* 21, PA1016, doi:10.1029/2004PA001112.

Algeo, T. J. and Scheckler, S. E., 1998. Terrestrial–marine teleconnections in the Devonian: links between the evolution of land plants, weathering processes, and marine anoxic events. *Phil. Trans*; 353, 113–130.

Algeo, T. J., and Shen, J., 2024. Theory and classification of mass extinction causation. *Natl. Sci. Rev.,* 11, nwad237. doi:10.1093/nsr/nwad237.

Algeo, T. J., Remírez, M. N., Zhao, H. Schwark, L., Gordon, G., Anbar, A., Bates, S., Lyons, T., Over, D.J., Sageman, B. B., 2025. Transient glacio-eustatic fall and its climato-environmental effects during the Frasnian-Famennian transition. *Glob. Planet. Change – this issue*.

Bennet, W. W., Canfield, D. E., 2020. Redox-sensitive trace metals as paleoredox proxies: A review and analysis of data from modern sediments. *Earth Sci. Rev.*; 204, 103175. https://doi.org/10.1016/j.earscirev.2020.103175.

Calvert, S. E. and Pedersen, T. F., 2007. Elemental proxies for palaeoclimatic and palaeoceanographic variability in marine sediments: interpretation and application. In: Hillaire-Marcel, C. and De Vernal, A. (Eds.) Proxies in late Cenozoic Paleoceanography, chapter 14, *Dev. In Mar. Geol.*; 1, 567-643. ISSN 1572-5480, doi:10.1016/S1572-5480(07)01019-6.

Carmichael, S. K., Waters, J. A., Königshof, P., Suttner, T. J., Kido, E., 2019. Paleogeography and paleoenvironments of the Late Devonian Kellwasser event: A review of its sedimentological and geochemical expression. *Glob. Planet. Change*; 183, 102984. https://doi.org/10.1016/j.gloplacha.2019.102984.

Chen, D., Wang, J., Racki, G., Li, H., Wang, C., Ma, X., Whalen, M. T., 2013. Large sulphur isotopic perturbations and oceanic changes during the Frasnian–Famennian transition of the Late Devonian. *J. Geol. Soc.*; 170, 465-476. https://doi.org/10.1144/jgs2012-037.

Chen, J., Lu, Y., Sun, Y., Hogancamp, N., Lu, M., 2024. Oceanic euxinia and seafloor oxygenation caused by continental weathering and influxes during the Late Devonian Frasnian-Famennian bio-crisis and Annulata bioevents. *Chem. Geol.*; 662, 122213. https://doi.org/10.1016/j.chemgeo.2024.122213.

Croudace, I. W. and Rothwell, R. G., 2015. Micro-XRF studies of sediment cores, Applications of a non-destructive tool for the environmental sciences. In: Smol, J. P. (Ed.), *Dev. in Paleoenv. Res.*; 17, ISSN 1571-5299.

De Vleeschouwer, D., Da Silva, A.-C., Sinnesael, M., Chen, D., Day, J. E., Whalen, M. T., Guo, Z., Claeys, P., 2017. Timing and pacing of the Late Devonian mass extinction event regulated by eccentricity and obliquity. *Nat. Comm.*; 8, 2268. doi:10.1038/s41467-017-02407-1.

Jaminski, J., Algeo, T.J., Maynard, J.B., Hower, J.C., 1998. Climatic origin of dm-scale compositional cyclicity in the Cleveland Member of the Ohio Shale (Upper Devonian), Central Appalachian Basin, USA. In: Schieber, J., et al. (eds.), *Shales and Mudstones*, *vol. 1*, Schweizerbart'sche, Stuttgart, Germany, 217-242.

Klapper, G. and Kirchgasser, W. T., 2016. Frasnian Late Devonian conodont biostratigraphy in New York: graphic correlation and taxonomy. *J. Paleontol.*; 90, 3, 525-55. doi: 10.1017/jpa.2015.70.

Liu, J.S., Algeo, T.J., Jaminski, J., Kuhn, T., Joachimski, M.M., 2019. Evaluation of high-frequency paleoenvironmental variation using an optimized cyclostratigraphic framework: Example for CS-Fe analysis of Devonian-Mississippian black shales (Central Appalachian Basin, USA). *Chem. Geol.*, *525*, 303-320.

Liu, J., Algeo, T.J., Hinnov, L.A., 2025. Identifying and quantifying stratigraphic disconformities in shale: An example from the Upper Devonian of the Appalachian Basin. *Geol. Soc. Am. Bull.*, 137, 20.

Lourens, L. J., Wehausen, R., Brumsack, H. J., 2001. Geological constraints on tidal dissipation and dynamical ellipticity of the Earth over the past three million years. *Nature*; 409, 1029-1033. https://doi.org/10.1038/35059062.

McLennan, S. M., 2001. Relationships between the trace element composition of sedimentary rocks and upper continental crust. *Geochem. Geophys. Geosyst.*; 2, 2000GC000109. https://doi.org/10.1029/2000GC000109.

Murphy, A. E., Sageman, B. B., Hollander, D. J., 2000. Eutrophication by decoupling of the marine biogeochemical cycles of C, N, and P: A mechanism for the Late Devonian mass extinction. *Geology*; 28, 5, 427-430.

Percival, L. M. E., Selby, D., Bond, D. P. G., Rakociński, M., Marynowski, L., Hood, A. v. S., Addate, T., Spangenberg, J. E., Föllmi, K. B., 2020. Phosphorus-cycle disturbances during the Late Devonian anoxic events. *Glob. Planet. Change*; 184, 103070. https://doi.org/10.1016/j.gloplacha.2019.103070.

Sageman, B. B., Murphy, A. E., Werne, J. P., Ver Straeten, C. A., Hollander, D. J., Lyons, T. W., 2003. A tale of shales: the relative roles of production, decomposition, and dilution in the accumulation of organic-rich strata, Middle–Upper Devonian, Appalachian basin. *Chem. Geol.*; 195, 229-273. doi:10.1016/S0009-2541(02)00397-2.

Smith, G. J. and Jacobi, R. D., 2023. Upper Frasnian and Famennian stratigraphy in western New York State. Chapter 3 in: Devonian of New York, Volume 3: Frasnian to Famennian (Upper Devonian) stages and the Devonian terrestrial system in New York, Ver Straeten, C.A., Over D. J., and Woodrow, D. (Eds.), *Bull. Am. Paleontol.;* 47-111. doi:10.32857/bap.2023.407.03.

Tribovillard, N., 2021. Re-assessing copper and nickel enrichments as paleoproductivity proxies. *Earth Sci. Bull.*; 192, 54. https://doi.org/10.1051/bsgf/2021047.

Tribovillard, N., Algeo, T. J., Lyons, T. W., Riboulleau, A., 2006. Trace metals as paleoredox and paleoproductivity proxies: An update. *Chem. Geol.*; 232, 12-32. doi:10.1016/j.chemgeo.2006.02.012.

Van der Weijden, C. H., 2002. Pitfalls of normalization of marine geochemical data using a common divisor. *Mar. Geol.*; 184, 167-187.

Ver Straeten, C. A., 2009. The classic Devonian of the Catskill Front: A foreland basin record of Acadian Orgenesis. In: Vollmer, F. (Ed), New York State Geological Association, 81st Annual Meeting Guidebook; 7, 1-54.

Ver Straeten, C. A., Brett, C. E., Sageman, B. B., 2011. Mudrock sequence stratigraphy: A multi-proxy (sedimentological, paleobiological and geochemical) approach, Devonian Appalachian Basin. *Palaeogeogr. Palaeoclimatol. Palaeoecol.*; 304, 54-73. doi:10.1016/j.palaeo.2010.10.010.

Whalen, M. T., De Vleeschouwer, D., Payne, J. H., Day, J. E., Over, D. J., Claeys, P., 2017. Pattern and timing of the Late Devonian biotic crisis in western Canada: Insights from carbon isotopes and astronomical calibration of magnetic susceptibility data. In: Playton, T. E., Kerans, C., Weissenberger, J. A. W. (Eds.). New advances in Devonian carbonates: Outcrop analogs, reservoirs and chronostratigraphy, *SEPM*; 107, 185-201. ISBN 978-1-56576-344-9. https://doi.org/10.2110/sepmsp.107

Wichern, N. M. A., Bialik, O. M., Nohl, T., Percival, L. M. E., Becker, T. R., Kaskes, P., Claeys, P., De Vleeschouwer, D., 2024. Astronomically paced climate and carbon cycle feedbacks in the lead-up to the Late Devonian Kellwasser Crisis. *Clim. Past;* 20, 415-448. https://doi.org/10.5194/cp-20-415-2024